



OPEN ACCESS

EDITED BY

Abderrahmen Merghni,
Tunis El Manar University, Tunisia

REVIEWED BY

Gerard Stephane,
Université de Reims Champagne-Ardenne,
France
Jing Cheng,
Envista, United States

*CORRESPONDENCE

Subhendu Bhowmik,
✉ sbhowmik@niperkolkata.ac.in

RECEIVED 20 April 2024

ACCEPTED 03 June 2024

PUBLISHED 26 June 2024

CITATION

Naithani K, Das A, Ushare M, Nath S, Biswas R, Kundu A, Ahmed KT, Mohan U and Bhowmik S (2024), Design, synthesis, and evaluation of 1,4-benzothiazine-3-one containing bisamide derivatives as dual inhibitors of *Staphylococcus aureus* with plausible application in a urinary catheter.

Front. Chem. 12:1420593.

doi: 10.3389/fchem.2024.1420593

COPYRIGHT

© 2024 Naithani, Das, Ushare, Nath, Biswas, Kundu, Ahmed, Mohan and Bhowmik. This is an open-access article distributed under the terms of the [Creative Commons Attribution License \(CC BY\)](https://creativecommons.org/licenses/by/4.0/). The use, distribution or reproduction in other forums is permitted, provided the original author(s) and the copyright owner(s) are credited and that the original publication in this journal is cited, in accordance with accepted academic practice. No use, distribution or reproduction is permitted which does not comply with these terms.

Design, synthesis, and evaluation of 1,4-benzothiazine-3-one containing bisamide derivatives as dual inhibitors of *Staphylococcus aureus* with plausible application in a urinary catheter

Kaushal Naithani¹, Arka Das¹, Mamta Ushare¹, Subham Nath^{1,2}, Rashmita Biswas^{1,2}, Anirban Kundu³, Kazi Tawsif Ahmed⁴, Utpal Mohan^{1,2} and Subhendu Bhowmik^{1*}

¹Department of Medicinal Chemistry, National Institute of Pharmaceutical Education and Research, Kolkata, West Bengal, India, ²Microbiology Division, Department of Medicinal Chemistry, National Institute of Pharmaceutical Education and Research, Kolkata, West Bengal, India, ³Department of Natural Product, National Institute of Pharmaceutical Education and Research, Kolkata, West Bengal, India, ⁴Department of Botany, Visva Bharati University, Santiniketan, West Bengal, India

In this study, 1,4-benzothiazine-based bisamide derivatives, a new class of antibacterial agents targeting bacterial peptide deformylase (PDF), were designed and synthesized to combat *Staphylococcus aureus* infection. Molecular modeling of the designed molecules showed better docking scores compared to the natural product actinonin. Bioactivity assessment identified two derivatives with promising antibacterial activity *in vitro*. The stability of the most active molecule, **8bE**, was assessed using molecular dynamics (MD) simulation. Significantly, compound **8bE** could also inhibit the *S. aureus* biofilm at low concentrations. Furthermore, the capability of the synthesized molecule to inhibit *S. aureus* biofilm formation on medical devices like urinary catheters is also demonstrated.

KEYWORDS

benzothiazine, *Staphylococcus aureus*, peptide deformylase, biofilm, catheter, computational studies

1 Introduction

Staphylococcus aureus, a Gram-positive bacterium that is mostly located in the upper respiratory tract and skin of healthy humans, is the major cause of nosocomial infection and is associated with significant mortality among hospitalized patients (Willekens et al., 2021). The major issue regarding *S. aureus* is its ability to form biofilms and grow on the surface of medical equipment like urinary catheters, which further increases the chances of infection among immune-compromised patients (de Oliveira et al., 2021). Catheter-associated UTIs (CAUTIs) are among the most frequent types of hospital-acquired infections and uropathogens like *S. aureus* (Walker et al., 2017). Biofilms are complex clusters of microorganisms produced by bacteria, providing the pathogens several advantages like resistance to phagocytosis and antimicrobial agents (Vashistha et al., 2023). On urinary catheters, the biofilms add another advantage to the bacteria as they provide resistance to

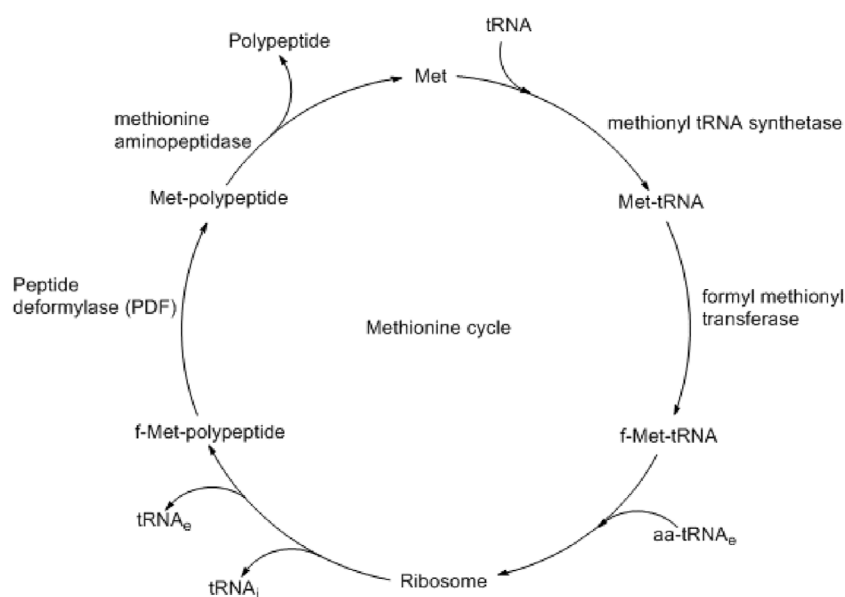


FIGURE 1 Methionine cycle shows the important role of peptide deformylase (PDF) in polypeptide synthesis (Aubart and Zalacain, 2006).

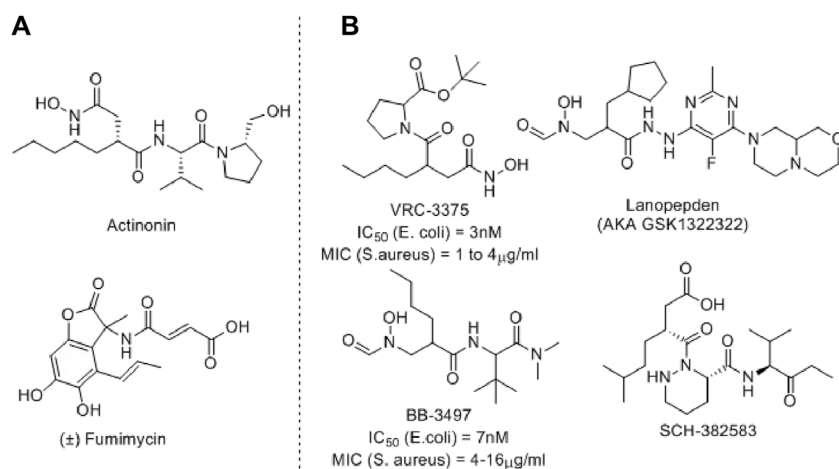


FIGURE 2 Representative examples of PDF inhibitors. (A) Naturally Occurring PDF inhibitors (B) PDF Inhibitors in clinical trials.

the bacteria against the sheer force of the urine flow (Werneburg, 2022). Therefore, the development of antibacterial agents that can inhibit bacterial biofilm formation on medical equipment is of utmost need.

Bacterial biofilm formation and pathogenesis are controlled by several enzymes like fibronectin-binding anchors and collagen-binding proteins (Foster et al., 2014). Some are responsible for virulence, and some are responsible for defense by biofilm formation. Although very challenging, the development of therapeutics by targeting both virulence and biofilm formation could be an effective option in controlling bacterial infection. Peptide deformylase (PDF) is one of such proteins present at the *def* gene of *S. aureus* and catalyzes the

deformylation step during protein synthesis (Margolis et al., 2000). During bacterial protein synthesis, N-formyl methionine, which is formed by formyl methionine tRNA transferase, is removed by PDF (Figure 1) (Aubart and Zalacain, 2006). Such a formylation–deformation cycle is essential for the growth and survival of all bacterial species, including *S. aureus* (Yang et al., 2014). Different studies also found that similar to the virulence proteins, the biosynthesis of biofilm-associated protein (Bap) also depends on such formylation–deformation steps, as controlled by PDF (Swarupa et al., 2018). Therefore, targeting PDF may prevent bacterial virulence and biofilm formation simultaneously.

Several PDF inhibitors have been developed so far using the natural product actinonin as a prototype, although none have been marketed (Figure 2). In all these known PDF inhibitors, the characteristic feature is the metal-binding hydroxamic or *N*-formylated or free acid site as the metal-binding motif (Yang et al., 2014). However, the robust metal-binding affinity of these groups creates toxicity by binding with the iron present in blood and, as a result, causes methemoglobinemia (Gokhale and Telvekar, 2021). To overcome this, other groups have developed thiol (Belete, 2019), *N*-substituted maleamic acid (Zaghouni et al., 2019), or peptide-based (Hu et al., 2004) PDF inhibitors, although with limited success. Keeping this in mind, herein, we designed a series of benzothiazine-3-one-based bisamide derivatives as plausible PDF inhibitors.

Benzothiazines are privileged scaffolds with numerous activities, including antibacterial, antifungal, and anticancer properties (Ahmad et al., 2014). Depending on the positioning of *N* and *S*-atoms, these scaffolds are classified as 1, 2-, 1,3-, or 1,4-benzothiazines. The 1,4-benzothiazines have antibacterial, antifungal, anticancer, and several other activities (Badshah and Naem, 2016). Furthermore, 1,4-benzothiazine-3-one containing hydroxamic acids also displayed good bacterial Ni-PDF inhibitory activity (Molteni et al., 2004). Considering such biological significance and known PDF inhibitory roles, we designed a 1,4-benzothiazine-3-one-containing molecule where the hydroxamic acid part is replaced with a bisamide side chain.

2 Materials and methods

2.1 Experimental section

Solvents were dried using standard procedures or collected from a solvent purification system (SPS). All starting materials were obtained from commercial suppliers and used as received. Products were purified by flash chromatography on silica gel (230–400 mesh, Merck). ¹H and ¹³C NMR spectra were recorded using JEOL-400-MHz instruments. Signals are quoted as δ values in ppm using residual protonated solvent signals as the internal standard (CDCl₃: δ 7.26 ppm). Data are reported as follows: chemical shift, multiplicity (*s* = singlet, *d* = doublet, *t* = triplet, *q* = quartet, *m* = multiplet, and *bs* = broad), coupling constants (Hz), and integration. The HRMS spectra were recorded as EI-HRMS (recorded as ESI+) using Q-TOF YA263 high-resolution (Water Corporation) instruments.

2.2 Chemistry

2.2.1 Synthesis and characterization

2.2.1.1 2-(3-Oxo-3,4-dihydro-2*H*-benzo[*b*][1,4]-thiazin-2-yl)-acetic acid (3)

Maleic anhydride (2) (4.3 g, 43.93 mM, 1.1 eq) was dissolved in toluene (~15 mL) and stirred until a clear solution was obtained. Then, 2-amino-thiophenol (1) (5 g, 39.94 mM, 1 eq) was added. The reaction was stirred for 6 h until an off-white precipitate was obtained. The precipitate was filtered off and washed with

CHCl₃. It was dried at room temperature to remove traces of CHCl₃. The precipitate was used without further purification. The desired compound was obtained as a white solid in 82% yield (7.13 g). Percentage yield = 82% as an off-white solid, *R*_f = 0.1 (hexane:EtOAc, 1:1); ¹H NMR (400 MHz, CD₃OD): δ 7.29 (d, *J* = 7.8 Hz, 1H), 7.18 (t, *J* = 7.6 Hz, 1H), 7.02 (t, *J* = 7.6 Hz, 1H), 6.97 (d, *J* = 7.8 Hz, 1H), 3.86 (dd, *J*₁ = 8 Hz, *J*₂ = 6.4 Hz, 1H), 2.91 (dd, *J*₁ = 16.4 Hz, *J*₂ = 6.3 Hz, 1H), and 2.52 (dd, *J*₁ = 16.4 Hz, *J*₂ = 6 Hz, 1H); ¹³C NMR (100 MHz, CD₃OD): δ 173.5, 168.6, 137.9, 129, 128.5, 124.9, 120.2, 118.4, 39.3, and 34.9 (Molteni et al., 2004).

2.2.1.2 General procedure for the synthesis of 8(aA–kG)

An amine derivative was dissolved in 5 mL reagent grade methanol and stirred until a clear solution was obtained. To this solution, carboxylic acid derivative, 3, was added, resulting in a suspension. This suspension was cooled to 5°C, and *tert*-butyl isocyanide, 7, was added. To this mixture, an aldehyde derivative was added, and the reaction was stirred at room temperature (~30°C) overnight.

NOTE: Reactions involving furfural aldehyde, tryptamine, or phenylethyl amine require a temperature of 60°C for the completion of the reaction.

Workup: The reaction mixture was evaporated until a solid layer was obtained. It was then dissolved in CHCl₃ and washed with distilled water (3*15 mL), followed by a brine solution (2*15 mL). The organic layer was then collected and dried using sodium sulfate. It was then evaporated in a rotavap until a thin film was obtained.

2.2.1.3 *N*-benzyl-*N*-[2-(*tert*-butylamino)-2-oxo-1-phenylethyl]-2-(3-oxo-3,4-dihydro-2*H*-benzo[*b*][1,4]-thiazin-2-yl)-acetamide (8aA)

The reaction was carried out as mentioned for the synthesis of 8. The desired compound was obtained as a pale-brown solid in 60% yield (135 mg), *R*_f = 0.3 (hexane:EtOAc, 7:3); ¹H NMR (400 MHz, CDCl₃): δ 8.77 (bs, 1H), 7.39–7.29 (m, 3H), 7.23–7.2 (m, 3H), 7.15–7.06 (m, 4H), 7.03–6.92 (m, 2H), 6.85–6.81 (m, 2H), 6.01–5.86 (m, 2H), 4.79–4.47 (m, 2H), 4.24–4.19 (m, 1H), 3.08–2.9 (m, 1H), 2.63–2.43 (m, 1H), 1.33 (s, 9H); ¹³C NMR (100 MHz, CDCl₃): δ 171.1, 168.7, 167.5, 137.1, 136, 134.8, 129.7, 128.5, 128.3, 128, 127.2, 126.8, 126, 125.8, 123.8, 119.7, 117.2, 63.2, 51.6, 49.8, 38.5, 33.4, and 28.6; ES + HRMS calculated for C₂₉H₃₁N₃O₃SNa = 524.1978 and obtained = 524.1997.

2.2.1.4 *N*-(4-Bromophenyl)-*N*-(2-(*tert*-butylamino)-2-oxo-1-phenylethyl)-2-(3-oxo-3,4-dihydro-2*H*-benzo[*b*][1,4]-thiazin-2-yl)-acetamide (8aC)

The reaction was carried out as mentioned for the synthesis of 8. The desired compound was obtained as a pale yellow solid in 54% yield (137 mg), *R*_f = 0.3 (hexane:EtOAc, 7:3); ¹H NMR (400 MHz, CDCl₃): δ 8.67 (s, 1H), 7.68 (s, 1H), 7.26 (dd, *J* = 7.79 Hz, 1.30 Hz, 1H), 7.20–7.10 (m, 6H), 6.98 (td, *J*₁ = 7.60 Hz, *J*₂ = 1.27 Hz, 1H), 6.82 (dd, *J*₁ = 7.95 Hz, *J*₂ = 1.07 Hz, 1H), 6.21–6.75 (m, 2H), 5.94–6.05 (m, 1H), 5.76–5.91 (m, 1H), 4.15 (dd, *J* = 8.02 Hz, 6.19 Hz, 1H), 2.76 (dd, *J* = 16.20 Hz, 6.19 Hz, 1H), 2.26 (q, *J* = 8.07 Hz, 1H), 1.31–1.36 (s, 9H); ¹³C NMR (100 MHz, CDCl₃): δ 169.8, 168.5, 167.3, 135.9, 134.3, 130.3, 128.4, 127.9, 127.3, 123.8, 119.5, 117.2, 65.5, 51.6, 38.5, 34.1, and 28.6; ES + HRMS calculated for C₂₈H₂₈BrN₃O₃SNa = 590.0912 and obtained = 590.0912.

2.2.1.5 *N*-(*tert*-butyl)-2-(*N*-(4-fluorophenyl)-2-[3-oxo-3,4-dihydro-2*H*-benzo[*b*][1,4]-thiazin-2-yl]-acetamido)-2-phenylacetamide (8aD)

The reaction was carried out as mentioned for the synthesis of 8. The desired compound was obtained as a gray solid in 51% yield (115 mg), $R_f = 0.3$ (hexane:EtOAc, 7:3); $^1\text{H NMR}$ (400 MHz, CDCl_3): δ 8.67 (s, 1H), 7.27 (d, $J = 1.4$ Hz, 1H), 7.25 (d, $J = 1.4$ Hz, 1H), 7.24–7.13 (m, 4H), 7.13–7.07 (m, 3H), 6.98 (td, $J_1 = 7.6$ Hz, $J_2 = 1.3$ Hz, 2H), 6.82 (dd, $J_1 = 8.0$ Hz, $J_2 = 1.1$ Hz, 1H), 6.00 (s, 1H), 5.85 (s, 1H), 4.15 (dd, $J_1 = 8.0$ Hz, $J_2 = 6.2$ Hz, 1H), 2.75 (dd, $J_1 = 16.2$ Hz, $J_2 = 6.2$ Hz, 1H), 2.26 (dd, $J_1 = 16.2$ Hz, $J_2 = 8.0$ Hz, 1H), 1.33 (s, 9H); $^{13}\text{C NMR}$ (100 MHz, CDCl_3): δ 169.8, 168.5, 167.3, 163.2, 160.7, 135.9, 135.2, 135.1, 134.3, 130.3, 128.4, 127.9, 127.3, 123.8, 119.5, 117.2, 65.5, 51.7, 38.5, 34.1, and 28.6; ES + HRMS calculated for $\text{C}_{28}\text{H}_{28}\text{FN}_3\text{O}_3\text{SNa} = 528.1733$ and obtained = 528.1727.

2.2.1.6 *N*-(*tert*-butyl)-2-(*N*-(3,5-dichlorophenyl)-2-(3-oxo-3,4-dihydro-2*H*-benzo[*b*][1,4]-thiazin-2-yl)-acetamido)-2-phenylacetamide (8aJ)

The reaction was carried out as mentioned for the synthesis of 8. The product was obtained as a white solid in 65% yield (162 mg), $R_f = 0.3$ (hexane:EtOAc, 7:3); $^1\text{H NMR}$ (400 MHz, $\text{DMSO}-d_6$): δ 10.57 (bs, 1H), 7.78 (s, 1H), 7.30 (d, $J = 7.6$ Hz, 2H), 7.25–7.13 (m, 4H), 7.05 (d, $J = 8.4$ Hz, 2H), 6.98 (t, $J = 7.2$ Hz, 2H), 6.87 (d, $J = 7.6$ Hz, 1H), 6.41 (bs, 1H), 6.03 (s, 1H), 3.82 (dd, $J_1 = 9.2$ Hz, $J_2 = 4.4$ Hz, 1H), 2.56–2.49 (m, 1H), 2.11–2.04 (m, 1H), 1.20 (s, 9H); $^{13}\text{C NMR}$ (100 MHz, $\text{DMSO}-d_6$): δ 168.38, 168.31, 165.9, 138.2, 136.6, 134.4, 132.5, 131.8, 131.5, 128.1, 127.9, 127.2, 123.2, 121.1, 117.8, 117.1, 63.0, 50.5, 38.0, 33.8, and 28.4; ES + HRMS calculated for $\text{C}_{28}\text{H}_{27}\text{Cl}_2\text{N}_3\text{O}_3\text{SNa} = 578.1048$ and obtained = 578.1040.

2.2.1.7 *N*-benzyl-*N*-(2-(*tert*-butylamino)-1-(4-nitrophenyl)-2-oxoethyl)-2-(3-oxo-3,4-dihydro-2*H*-benzo[*b*][1,4]-thiazin-2-yl)-acetamide (8bA)

The reaction was carried out as mentioned for the synthesis of 8. The desired compound was obtained as a pale yellow solid in 60% yield (147 mg), $R_f = 0.3$ (hexane:EtOAc, 7:3); $^1\text{H NMR}$ (400 MHz, CDCl_3): δ 8.23 (d, $J = 8.4$ Hz, 2H), 8.09 (d, $J = 31.5$ Hz, 2H), 7.69 (d, $J = 8.4$ Hz, 2H), 7.49 (d, $J = 7.5$ Hz, 1H), 7.36–7.30 (m, 2H), 7.19 (d, $J = 7.0$ Hz, 1H), 7.08 (dt, $J_1 = 13$ Hz, $J_2 = 7.5$ Hz, 3H), 6.35 (d, $J = 26.5$ Hz, 1H), 4.68 (d, $J = 18.0$ Hz, 2H), 4.33–4.18 (m, 1H), 3.17 (dd, $J_1 = 16.1$ Hz, $J_2 = 5.3$ Hz, 1H), 2.90 (dd, $J_1 = 16.1$ Hz, $J_2 = 8.6$ Hz, 1H), 1.49 (s, 9H); $^{13}\text{C NMR}$ (100 MHz, CDCl_3): δ 171.8, 168.7, 167.3, 147.6, 142.9, 137, 136.4, 130.5, 128.1, 127.8, 127.1, 126.8, 125.7, 123.7, 122.9, 120.1, 117.1, 113.2, 62.1, 51.3, 49.2, 38.7, 33.4, and 27.4; ES + HRMS calculated for $\text{C}_{29}\text{H}_{30}\text{N}_4\text{O}_5\text{SNa} = 569.1829$ and obtained = 569.1842.

2.2.1.8 *N*-(*tert*-butyl)-2-[*N*-(3-chlorophenyl)-2-(3-oxo-3,4-dihydro-2*H*-benzo[*b*][1,4]-thiazin-2-yl)-acetamido]-2-(4-nitrophenyl)-acetamide (8bB)

The reaction was carried out as mentioned for the synthesis of 8. The desired compound was obtained as a greyish white solid in 55% yield (140 mg), $R_f = 0.3$ (hexane:EtOAc, 7:3); $^1\text{H NMR}$ (400 MHz, CDCl_3): δ 8.86 (bs, 1H), 8.02 (d, $J = 7.2$ Hz, 2H), 7.38 (d, $J = 8.4$ Hz, 2H), 7.29–7.27 (m, 2H), 7.21 (d, $J = 6.8$ Hz, 1H), 7.14–7.10 (m, 2H), 7.03–6.9 (m, 2H), 6.82 (d, $J = 8$ Hz, 1H), 6.19 (s, 1H), 5.99 (bs, 1H),

4.15–4.11 (m, 1H), 2.7 (q, $J = 8$ Hz, 1H), 2.32 (dd, $J_1 = 16$ Hz, $J_2 = 6.4$ Hz, 1H), 1.36 (s, 9H); $^{13}\text{C NMR}$ (100 MHz, CDCl_3): δ 170, 167.3, 147.6, 141.4, 140.1, 135.8, 131.1, 130.3, 129.2, 128.5, 128, 127.4, 124.1, 123.3, 119.7, 117.2, 64.8, 52, 38.4, 33.9, and 28.6; ES + HRMS calculated for $\text{C}_{28}\text{H}_{27}\text{ClN}_4\text{O}_5\text{S} = 567.1361$ and obtained = 567.1359.

2.2.1.9 *N*-(4-bromophenyl)-*N*-(2-(*tert*-butylamino)-1-(4-nitrophenyl)-2-oxoethyl)-2-(3-oxo-3,4-dihydro-2*H*-benzo[*b*][1,4]-thiazin-2-yl)-acetamide (8bC)

The reaction was carried out as mentioned for the synthesis of 8. The product was obtained as a pale yellow solid in 58% yield (148 mg), $R_f = 0.3$ (hexane:EtOAc, 7:3); $^1\text{H NMR}$ (400 MHz, CDCl_3): δ 8.07–8.05 (m, 3H), 7.47–7.27 (m, 6H), 7.17 (t, $J = 7.6$ Hz, 1H), 7.01 (t, $J = 8$ Hz, 1H), 6.82 (d, $J = 8$ Hz, 1H), 6.32 (bs, 1H), 6.16 (s, 1H), 4.17 (d, $J = 6$ Hz, 2 Hz, 1H), 2.69 (dd, $J_1 = 8.4$ Hz, $J_2 = 7.6$ Hz, 1H), 2.28 (dd, $J_1 = 10$ Hz, $J_2 = 6$ Hz), and 1.39 (s, 9H); $^{13}\text{C NMR}$ (100 MHz, CDCl_3): δ 170.1, 167.3, 167.1, 147.6, 141.5, 137.9, 135.8, 132.6, 131.8, 131.5, 131.3, 127.9, 127.4, 124, 123.4, 119.8, 117.2, 64.4, 52, 38.5, 33.8, and 28.6; ES + HRMS calculated for $\text{C}_{28}\text{H}_{27}\text{BrN}_4\text{O}_5\text{SNa} = 633.0783$ and obtained = 633.0812.

2.2.1.10 *N*-(*tert*-butyl)-2-(*N*-(4-fluorophenyl)-2-(3-oxo-3,4-dihydro-2*H*-benzo[*b*][1,4]-thiazin-2-yl)-acetamido)-2-(4-nitrophenyl)-acetamide (8bD)

The reaction was carried out as mentioned for the synthesis of 8. The desired compound was obtained as a pale white solid in 56% yield (138 mg), $R_f = 0.3$ (hexane:EtOAc, 7:3); $^1\text{H NMR}$ (400 MHz, CDCl_3): δ 8.28 (s, 1H), 8.04 (d, $J = 8.86$ Hz, 2H), 7.35 (d, $J = 8.75$ Hz, 2H), 7.28 (d, $J = 1.26$ Hz, 1H), 7.17–7.13 (m, 1H), 7.00 (td, $J_1 = 7.63$ Hz, $J_2 = 1.24$ Hz, 1H), 6.82 (dd, $J_1 = 7.95$ Hz, $J_2 = 0.86$ Hz, 1H), 6.35 (s, 1H), 6.16 (s, 1H), 4.16 (dd, $J = 7.98$ Hz, 6.37 Hz, 1H), 2.70 (q, $J = 7.97$ Hz, 1H), 2.28 (dd, $J_1 = 15.87$ Hz, $J_2 = 6.32$ Hz, 1H), and 1.38 (s, 9H); $^{13}\text{C NMR}$ (100 MHz, CDCl_3): δ 170.4, 167.4, 167.1, 147.6, 141.6, 135.8, 131.8, 131.7, 131.3, 127.9, 127.5, 124.0, 123.3, 117.2, 64.4, 52.0, 38.5, 33.8, and 28.6; ES + HRMS calculated for $\text{C}_{28}\text{H}_{27}\text{FN}_4\text{O}_5\text{SNa} = 551.1686$ and obtained = 551.1653.

2.2.1.11 *N*-(2-(1*H*-indol-3-yl)-ethyl)-*N*-(2-(*tert*-butylamino)-1-(4-nitrophenyl)-2-oxoethyl)-2-(3-oxo-3,4-dihydro-2*H*-benzo[*b*][1,4]-thiazin-2-yl)-acetamide (8bE)

The reaction was carried out as mentioned for the synthesis of 8. The desired compound was obtained as a greyish white solid in 64% yield (172 mg), $R_f = 0.15$ (hexane:EtOAc, 7:3); $^1\text{H NMR}$ (400 MHz, CDCl_3): δ : 8.42–8 (m, 4H), 7.63–7.57 (m, 2H), 7.31–7.29 (m, 2H), 7.16–7.01 (m, 4H), 6.85–6.77 (m, 2H), 6.47 (bs, 1H), 5.89 (s, 1H), 4.24–4.19 (m, 1H), 3.86–3.50 (m, 2H), and 3.12–2.50 (m, 4H); $^{13}\text{C NMR}$ (100 MHz, CDCl_3): δ 170.9, 167.8, 167.2, 147.4, 143.1, 136.1, 135.9, 130.0, 129.6, 128.0, 127.5, 126.7, 125.0, 124.2, 123.6, 122.3, 122.1, 120.0, 119.7, 118.2, 117.2, 111.5, 111.3, 63.3, 51.9, 48.4, 38.6, 32.7, 31.9, and 28.6; ES + HRMS calculated for $\text{C}_{32}\text{H}_{33}\text{N}_5\text{O}_5\text{SNa} = 622.2055$ and obtained = 622.2056.

2.2.1.12 *N*-(*tert*-butyl)-2-(4-nitrophenyl)-2-(2-(3-oxo-3,4-dihydro-2*H*-benzo[*b*][1,4]-thiazin-2-yl)-*N*-phenethylacetamido)-acetamide (8bF)

The reaction was carried out as mentioned for the synthesis of 8. The product was obtained as a gray solid in 60% yield (151 mg), $R_f =$

0.2 (hexane:EtOAc, 7:3); ^1H NMR (400 MHz, CDCl_3): δ 8.82 (bs, 1H), 8.25–8.14 (m, 3H), 7.62 (dd, $J_1 = 10.8$ Hz, $J_2 = 8.8$ Hz, 2H), 7.3 (t, $J = 6.8$ Hz, 1H), 7.19–7.14 (m, 5H), 7.03–6.99 (m, 1H), 6.89–6.84 (m, 3H), 6.52 (bs, 1H), 5.99 (s, 1H), 4.22 (t, $J = 7$ Hz, 1H), 3.70–3.47 (m, 2H), 3.13–3.06 (m, 1H), 2.91–2.31 (m, 3H), and 1.39 (s, 9H); ^{13}C NMR (100 MHz, CDCl_3): δ 170.8, 167.6, 167.3, 147.5, 143.0, 137.3, 137.1, 135.9, 129.9, 129.6, 128.7, 128.4, 128.0, 127.5, 127.1, 126.8, 124.2, 123.9, 123.7, 119.7, 117.3, 62.9, 51.9, 49.2, 38.7, 36.6, 32.5, and 28.5; ES + HRMS calculated for $\text{C}_{30}\text{H}_{32}\text{N}_4\text{O}_5\text{S}$ = 561.2093 and obtained = 561.2061.

2.2.1.13 *N*-(*tert*-butyl)-2-(*N*-(4-hydroxyphenyl)-2-(3-oxo-3,4-dihydro-2*H*-benzo[*b*][1,4]-thiazin-2-yl)-acetamido)-2-(4-nitrophenyl)-acetamide (8bl)

The reaction was carried out as mentioned for the synthesis of 8. The product was obtained as a pale brown solid in 55% yield (155 mg), $R_f = 0.1$ (hexane:EtOAc, 7:3); ^1H NMR (400 MHz, CDCl_3): δ 8.06–8.03 (m, 3H), 7.43–7.27 (m, 3H), 7.18–7.13 (m, 1H), 7.03–6.99 (m, 1H), 6.81–6.78 (m, 1H), 6.52–6.29 (m, 2H), 6.14–5.94 (m, 2H), 4.19–4.10 (m, 1H), 2.80–2.72 (m, 1H), 2.34–2.23 (m, 1H), and 1.40 (s, 9H); ^{13}C NMR (100 MHz, CDCl_3): δ 170.9, 168.0, 167.4, 156.6, 147.5, 141.7, 135.7, 131.2, 131.1, 131.0, 130.9, 130.8, 127.9, 127.4, 124.1, 123.2, 120.0, 117.3, 116.2, 65.3, 52.1, 38.4, 33.7, and 28.6; ES + HRMS calculated for $\text{C}_{28}\text{H}_{28}\text{N}_4\text{O}_6\text{SNa}$ = 571.1627 and obtained = 571.1631.

2.2.1.14 *N*-(4-bromophenyl)-*N*-(2-(*tert*-butylamino)-1-(4-chlorophenyl)-2-(3-oxo-3,4-dihydro-2*H*-benzo[*b*][1,4]-thiazin-2-yl)-acetamido)-acetamide (8cC)

The reaction was carried out as mentioned for the synthesis of 8. The product was obtained as a pale white solid in 52% yield (140 mg), $R_f = 0.3$ (hexane:EtOAc, 7:3); ^1H NMR (400 MHz, CDCl_3): δ 8.96 (d, $J = 9.38$ Hz, 1H), 7.28 (dd, $J_1 = 7.86$ Hz, $J_2 = 1.34$ Hz, 1H), 7.14–7.08 (m, 4H), 7.05 (d, $J = 8.52$ Hz, 2H), 6.99 (td, $J_1 = 7.58$, $J_2 = 1.26$ Hz, 1H), 6.82 (d, $J = 7.78$ Hz, 1H), 5.96 (d, $J = 18.52$ Hz, 2H), 4.09–4.18 (m, 1H), 2.68 (dd, $J_1 = 16.09$ Hz, $J_2 = 7.46$ Hz, 1H), 2.27 (dd, $J_1 = 16.07$ Hz, $J_2 = 6.58$ Hz, 1H), and 1.32 (s, 9H); ^{13}C NMR (100 MHz, CDCl_3): δ 170.0, 168.2, 167.4, 135.9, 134.4, 132.8, 132.1, 132.0, 131.6, 128.5, 127.8, 127.3, 123.8, 119.3, 117.3, 64.5, 51.7, 38.5, 34.0, and 28.5; ES + HRMS calculated for $\text{C}_{28}\text{H}_{27}\text{BrClN}_3\text{O}_3\text{SNa}$ = 622.0543 and obtained = 622.0554.

2.2.1.15 *N*-(*tert*-butyl)-2-(4-chlorophenyl)-2-(*N*-(4-fluorophenyl)-2-(3-oxo-3,4-dihydro-2*H*-benzo[*b*][1,4]-thiazin-2-yl)-acetamido)-acetamide (8cD)

The desired compound was obtained as a pale white solid in 51% yield (121 mg), $R_f = 0.2$ (hexane:EtOAc, 7:3); ^1H NMR (400 MHz, CDCl_3): δ 8.06 (d, $J = 24.53$ Hz, 1H), 7.28 (d, $J = 1.07$ Hz, 1H), 7.19–7.13 (m, 3H), 7.07 (d, $J = 8.48$ Hz, 1H), 7.00 (td, $J_1 = 7.60$ Hz, $J_2 = 1.20$ Hz, 1H), 6.80 (dd, $J_1 = 7.95$ Hz, $J_2 = 1$ Hz, 1H), 5.99 (d, $J = 4.28$ Hz, 1H), 4.15 (t, $J = 7.11$ Hz, 1H), 2.72 (dd, $J_1 = 16.09$ Hz, $J_2 = 7.22$ Hz, 1H), 2.25 (dd, $J_1 = 16.05$ Hz, $J_2 = 7.03$ Hz, 1H), and 1.35 (s, 9H); ^{13}C NMR (100 MHz, CDCl_3): δ 169.8, 168.0, 167.0, 138.1, 135.8, 134.5, 132.8, 131.9, 131.7, 128.6, 128.0, 127.4, 123.9, 119.8, 117.1, 64.5, 51.8, 38.5, 33.9, and 28.6; ES + HRMS calculated for $\text{C}_{28}\text{H}_{27}\text{ClFN}_3\text{O}_3\text{SNa}$ = 562.1343 and obtained = 562.1328.

2.2.1.16 *N*-(2-(1*H*-indol-3-yl)-ethyl)-*N*-(2-(*tert*-butylamino)-1-(4-chlorophenyl)-2-oxoethyl)-2-(3-oxo-3,4-dihydro-2*H*-benzo[*b*][1,4]-thiazin-2-yl)-acetamide (8cE)

The reaction was carried out as mentioned for the synthesis of 8. The desired compound was obtained as an off-white solid in 62% yield (mg), $R_f = 0.25$ (hexane:EtOAc, 7:3); ^1H NMR (400 MHz, CDCl_3): δ 8.73 (bs, 1H), 7.44–7.29 (m, 5H), 7.19–7.14 (m, 4H), 7.02–6.91 (m, 1H), 6.90–6.76 (m, 1H), 6.21–5.94 (m, 2H), 4.25 (q, $J = 8.8$ Hz, 1H), 3.58–3.40 (m, 2H), 3.12–3.08 (m, 1H), 2.74–2.49 (m, 2H), 2.23–2.15 (m, 1H), and 1.36 (s, 9H); ^{13}C NMR (100 MHz, CDCl_3): δ 170.4, 168.3, 167.4, 137.7, 135.9, 134.4, 134.2, 133.9, 131.1, 130.8, 128.9, 128.6, 128.4, 128.1, 127.5, 126.7, 126.6, 124.2, 119.7, 117.2, 61.9, 51.7, 48.3, 38.7, 36.3, 32.7, and 28.6; ES + HRMS calculated for $\text{C}_{32}\text{H}_{33}\text{ClN}_4\text{O}_3\text{SNa}$ = 611.1854 and obtained = 611.1864.

2.2.1.17 *N*-(*tert*-butyl)-2-(4-chlorophenyl)-2-(2-(3-oxo-3,4-dihydro-2*H*-benzo[*b*][1,4]-thiazin-2-yl)-*N*-phenethylacetamido)-acetamide (8cF)

The reaction was carried out as mentioned for the synthesis of 8. The product was obtained as a white solid in 55% yield (134 mg), $R_f = 0.25$ (hexane:EtOAc, 7:3); ^1H NMR (400 MHz, CDCl_3): δ 9.16 (bs, 1H), 8.25 (s, 1H), 7.41–7.28 (m, 5H), 7.13–7.11 (m, 3H), 7.04–6.94 (m, 2H), 6.90–6.87 (m, 1H), 6.63 (dd, $J_1 = 10$ Hz, $J_2 = 2$ Hz, 1H), 6.24 (bs, 1H), 5.93 (s, 1H), 4.23–4.19 (m, 1H), 3.62–3.47 (m, 2H), 3.08–2.56 (m, 3H), 2.46–2.40 (m, 1H), and 1.36 (s, 9H); ^{13}C NMR (100 MHz, CDCl_3): δ 170.5, 168.6, 167.5, 136.0, 134.4, 134.1, 133.9, 130.9, 128.9, 127.9, 127.4, 126.8, 124.0, 122.0, 119.5, 118.2, 117.3, 111.7, 111.2, 62.5, 51.7, 47.5, 38.6, 32.8, 28.6, and 25.8; ES + HRMS calculated for $\text{C}_{30}\text{H}_{32}\text{ClN}_3\text{O}_3\text{S}$ = 550.1811 and obtained = 550.1816.

2.2.1.18 *N*-(*tert*-butyl)-2-(4-chlorophenyl)-2-(*N*-(4-hydroxyphenyl)-2-(3-oxo-3,4-dihydro-2*H*-benzo[*b*][1,4]-thiazin-2-yl)-acetamido)-acetamide (8cI)

The reaction was carried out as mentioned for the synthesis of 8. The product was obtained as an off-white solid with 55% yield (108 mg), $R_f = 0.1$ (hexane:EtOAc, 7:3); ^1H NMR (400 MHz, CDCl_3): δ 9.07 (bs, 1H), 7.35–7.26 (m, 1H), 7.20 (d, $J = 7.6$ Hz, 1H), 7.12–7.04 (m, 5H), 6.95 (t, $J = 7.4$ Hz, 1H), 6.82–6.39 (m, 3H), 6.21 (bs, 1H), 5.87 (s, 1H), 4.14–4.07 (m, 1H), 2.80–2.71 (m, 1H), 2.36–2.27 (m, 1H), and 1.31 (s, 9H); ^{13}C NMR (100 MHz, CDCl_3): δ 170.8, 168.8, 167.6, 156.7, 135.7, 134.3, 132.9, 131.6, 130.8, 128.4, 127.8, 127.3, 123.9, 119.6, 117.4, 60.5, 51.9, 51.8, 38.4, and 28.5; ES + HRMS calculated for $\text{C}_{28}\text{H}_{28}\text{ClN}_3\text{O}_4\text{SNa}$ = 560.1387 and obtained = 560.1390.

2.2.1.19 *N*-(*tert*-butyl)-2-(furan-2-yl)-2-(*N*-(4-methoxyphenyl)-2-(3-oxo-3,4-dihydro-2*H*-benzo[*b*][1,4]-thiazin-2-yl)-acetamido)-acetamide (8dG)

The reaction was carried out as mentioned for the synthesis of 8. The desired compound was obtained as a pale brown solid in 48% yield (109 mg), $R_f = 0.25$ (hexane:EtOAc, 7:3); ^1H NMR (400 MHz, CDCl_3): δ 8.86 (bs, 1H), 7.28–7.25 (m, 3H), 7.12–7.10 (m, 1H), 7.00–6.98 (m, 1H), 6.83–6.81 (m, 1H), 6.72–6.56 (m, 2H), 6.30–6.25 (m, 2H), 6.18–6.15 (m, 2H), 4.16–4.11 (m, 1H), 3.73 (s, 3H), 2.78–2.71 (m, 1H), 2.35–2.27 (m, 1H), and 1.37 (s, 9H); ^{13}C

NMR (100 MHz, CDCl₃): δ 170.3, 167.5, 166.5, 159.3, 147.8, 142.3, 135.9, 131.6, 127.9, 127.2, 123.7, 119.8, 117.2, 114.2, 112.1, 112.0, 110.6, 59.0, 55.3, 51.6, 38.5, 33.7, and 28.6; ES + HRMS calculated for C₂₇H₂₉N₃O₅S = 508.1861 and obtained = 508.1854.

2.2.1.20 *N*-(*tert*-butyl)-2-(furan-2-yl)-2-(*N*-(4-nitrophenyl)-2-(3-oxo-3,4-dihydro-2*H*-benzo[*b*][1,4]-thiazin-2-yl)-acetamido)-acetamide (8dH)

The reaction was carried out as mentioned for the synthesis of 8. The desired compound was obtained as a reddish brown solid in 48% yield (112 mg), R_f = 0.3 (hexane:EtOAc, 7:3); ¹H NMR (400 MHz, CDCl₃): δ 8.06 (m, 3H), 7.86 (s, 1H), 7.30–7.26 (m, 2H), 7.17–7.13 (m, 1H), 7.03–6.98 (m, 1H), 6.77 (d, J = 8.00 Hz, 1H), 6.30–6.17 (m, 3H), 6.04 (s, 1H), 4.16 (t, J = 7.06 Hz, 1H), 2.71 (dd, J_1 = 16.07 Hz, J_2 = 7.09 Hz, 1H), 2.28 (dd, J = 16.04 Hz, 7.06 Hz, 1H), and 1.37 (s, 9H); ¹³C NMR (100 MHz, CDCl₃): δ 169, 167.2, 166.1, 147.3, 146.9, 145.0, 143.2, 135.8, 131.2, 128.0, 127.3, 124.1, 124.0, 119.7, 117.2, 112.6, 110.8, 58.9, 51.9, 38.2, 33.8, 29.7, and 28.5; ES + HRMS calculated for C₂₆H₂₆N₄O₆SNa = 545.1471 and obtained = 545.1484.

2.2.1.21 *N*-(4-bromophenyl)-*N*-(2-(*tert*-butylamino)-2-oxo-1-(*m*-tolyl)-ethyl)-2-(3-oxo-3,4-dihydro-2*H*-benzo[*b*][1,4]-thiazin-2-yl)-acetamide (8eC)

The reaction was carried out as mentioned for the synthesis of 8. The product was obtained as a pale yellow solid in 52% yield (135 mg), R_f = 0.3 (30% EtOAc in hexane); ¹H NMR (400 MHz, CDCl₃): δ 8.42 (s, 1H), 7.43–7.27 (m, 1H), 7.13 (td, J = 7.7, 1.4 Hz, 1H), 7.06 (t, J = 7.5 Hz, 1H), 7.02–6.96 (m, 3H), 6.93 (s, 1H), 6.89 (d, J = 7.5 Hz, 2H), 6.80 (d, J = 7.9 Hz, 2H), 5.94 (s, 1H), 5.82 (s, 1H), 4.21–4.11 (m, 1H), 2.77 (dd, J = 16.2 Hz, 6.3 Hz, 1H), 2.26 (dd, J = 16.3 Hz, 7.9 Hz, 1H), 2.22 (s, 3H), and 1.34 (s, 9H); ¹³C NMR (100 MHz, CDCl₃): δ 169.8, 168.6, 167.3, 138.0, 135.8, 135.3, 134.2, 132.1, 131.0, 129.1, 128.2, 127.9, 127.3, 123.8, 119.7, 117.1, 65.6, 51.6, 38.5, 34.0, 28.6, and 21.2; ES + HRMS calculated for C₂₉H₃₀BrN₃O₃S = 580.1225 and obtained = 580.1200.

2.2.1.22 *N*-(*tert*-butyl)-2-(*N*-(4-fluorophenyl)-2-(3-oxo-3,4-dihydro-2*H*-benzo[*b*][1,4]-thiazin-2-yl)-acetamido)-2-(*m*-tolyl)-acetamide (8eD)

The reaction was carried out as mentioned for the synthesis of 8. The desired compound was obtained as a pale-brown solid in 55% yield (127 mg), R_f = 0.3 (hexane:EtOAc, 7:3); ¹H NMR (400 MHz, CDCl₃): δ 8.69 (s, 1H), 7.25 (d, J = 1.30 Hz, 1H), 7.13 (t, J = 7.68 Hz, 1H), 7.08–6.96 (m, 3H), 6.94 (s, 1H), 6.89 (d, J = 7.41 Hz, 1H), 6.82 (dd, J_1 = 7.99 Hz, J_2 = 1.11 Hz, 1H), 5.93 (s, 1H), 5.80 (s, 1H), 4.15 (dd, J_1 = 7.91 Hz, J_2 = 6.23 Hz, 1H), 2.77 (dd, J_1 = 16.24 Hz, J_2 = 6.23 Hz, 1H), 2.28–2.22 (m, 4H), and 1.32 (s, 9H); ¹³C NMR (100 MHz, CDCl₃): δ 169.8, 168.7, 167.5, 163.2, 160.7, 138.0, 136.0, 135.2, 134.1, 132.4, 131.0, 129.1, 128.2, 127.9, 127.3, 123.8, 120.0, 117.1, 115.7, 115.5, 65.4, 51.6, 38.3, 28.6, and 21.2; ES + HRMS calculated for C₂₉H₃₀FN₃O₃SNa = 542.1890 and obtained = 542.1899.

2.2.1.23 *N*-(2-(1*H*-indol-3-yl)-ethyl)-*N*-(2-(*tert*-butylamino)-1-(2-nitrophenyl)-2-oxoethyl)-2-(3-oxo-3,4-dihydro-2*H*-benzo[*b*][1,4]-thiazin-2-yl)-acetamide (8fE)

The reaction was carried out as mentioned for the synthesis of 8. The desired compound was obtained as a pale brown solid in 59%

yield (158 mg), R_f = 0.15 (hexane:EtOAc, 7:3); ¹H NMR (400 MHz, CDCl₃): δ 8.5–8.18 (m, 3H), 7.63 (dd, J_1 = 8.4 Hz, J_2 = 2.4 Hz, 2H), 7.33–7.3 (m, 1H), 7.22–7.17 (m, 4H), 7.02 (t, J = 7.6 Hz, 1H), 6.91–6.87 (m, 3H), 6.43 (bs, 1H), 5.95 (s, 1H), 4.26–4.21 (m, 1H), 3.71–3.48 (m, 2H), 3.14–3.07 (m, 2H), 2.93–2.38 (m, 3H), and 1.40 (s, 9H); ¹³C NMR (100 MHz, CDCl₃): δ 170.8, 167.6, 167.3, 147.5, 143.1, 137.2, 135.9, 130, 129.7, 128.7, 128.5, 128.1, 127.6, 126.9, 124.2, 123.7, 117.3, 63.0, 51.9, 49.2, 38.7, 36.1, 32.5, and 28.6; ES + HRMS calculated for C₃₂H₃₃N₅O₅SNa = 622.2094 and obtained = 622.2103.

2.2.1.24 *N*-(2-(1*H*-indol-3-yl)-ethyl)-*N*-(2-(*tert*-butylamino)-1-(3-nitrophenyl)-2-oxoethyl)-2-(3-oxo-3,4-dihydro-2*H*-benzo[*b*][1,4]-thiazin-2-yl)-acetamide (8gE)

The reaction was carried out as mentioned for the synthesis of 8. The desired compound was obtained as a pale brown solid in 55% yield (148 mg), R_f = 0.15 (hexane:EtOAc, 7:3); ¹H NMR (400 MHz, CDCl₃): δ 8.20–8.05 (m, 3H), 7.60 (q, J = 7.2 Hz, 2H), 7.31–7.28 (m, 2H), 7.16–7.01 (m, 5H), 6.86–6.80 (m, 2H), 6.43 (bs, 1H), 5.91 (s, 1H), 4.24–4.19 (m, 1H), 3.81–3.54 (m, 2H), 3.12–2.51 (m, 4H), and 1.39 (s, 9H); ¹³C NMR (100 MHz, CDCl₃): δ 170.9, 167.9, 167.3, 148.1, 137.9, 137.7, 136.0, 135.8, 135.2, 134.9, 134.3, 129.4, 127.9, 127.4, 124.1, 123.8, 122.9, 122.1, 119.5, 119.3, 118.0, 117.5, 111.3, 62.6, 53.4, 47.9, 38.7, 32.6, 30.8, and 28.5; ES + HRMS calculated for C₃₂H₃₃N₅O₅SNa = 622.2100 and obtained = 622.2110.

2.2.1.25 *N*-benzyl-*N*-(2-(*tert*-butylamino)-2-oxo-1-(*p*-tolyl)-ethyl)-2-(3-oxo-3,4-dihydro-2*H*-benzo[*b*][1,4]-thiazin-2-yl)-acetamide (8hA)

The reaction was carried out as mentioned for the synthesis of 8. The desired compound was obtained as an off-white solid in 65% yield (150 mg), R_f = 0.3 (hexane:EtOAc, 7:3); ¹H NMR (400 MHz, CDCl₃): δ 9.25 (bs, 1H), 7.30–7.28 (m, 1H), 7.25–7.22 (m, 2H), 7.10–7.06 (m, 5H), 7.01–6.91 (m, 3H), 6.87–6.82 (m, 2H), 5.99–5.92 (m, 2H), 4.75–4.35 (m, 2H), 4.21–4.17 (m, 1H), 3.08–2.88 (m, 1H), 2.50–2.44 (m, 1H), 2.25 (s, 3H), and 1.31 (s, 9H); ¹³C NMR (100 MHz, CDCl₃): δ 171.2, 168.9, 167.5, 138.2, 137.2, 135.9, 131.8, 129.7, 129.5, 129.2, 128.6, 128.3, 128, 128, 127.4, 127.2, 126.8, 126.1, 125.9, 123.8, 117.2, 117.1, 63.3, 51.6, 49.7, 38.6, 38.4, 33.5, 28.6, and 21; ES + HRMS calculated for C₃₀H₃₃N₃O₃SNa = 538.2135 and obtained = 538.2151.

2.2.1.26 *N*-benzyl-*N*-(2-(*tert*-butylamino)-1-(4-methoxyphenyl)-2-oxoethyl)-2-(3-oxo-3,4-dihydro-2*H*-benzo[*b*][1,4]-thiazin-2-yl)-acetamide (8iA)

The reaction was carried out as mentioned for the synthesis of 8. The desired compound was obtained as a pale brown solid in 62% yield (147 mg), R_f = 0.3 (hexane:EtOAc, 7:3); ¹H NMR (400 MHz, CDCl₃): δ 9.23 (bs, 1H), 7.27–7.26 (m, 2H), 7.25–7.24 (m, 1H), 7.13–7.06 (m, 4H), 7.01–6.96 (m, 1H), 6.94–6.91 (m, 1H), 6.88–6.83 (m, 2H), 6.73–6.67 (m, 2H), 6.01–5.83 (m, 2H), 4.75–4.44 (m, 2H), 4.22–4.09 (m, 1H), 3.70 (s, 3H), 3.09–2.88 (m, 1H), 2.61–2.44 (m, 1H), and 1.32 (s, 9H); ¹³C NMR (100 MHz, CDCl₃): δ 171.3, 171.1, 169, 169, 167.6, 159.5, 137.3, 137.2, 136.1, 135.9, 131.1, 131, 128.3, 127.9, 127.2, 127.2, 126.8, 126.7, 126.7, 126, 125.8, 123.8, 123.8, 119.9, 119.4, 117.3, 117.2, 113.9, 113.9, 99.9, 62.8, 62.4, 60.4, 55.2, 51.5, 49.5, 38.5, 38.3, 33.5, 33.4, and 28.6; ES + HRMS calculated for C₃₀H₃₃N₃O₄SNa = 554.2084 and obtained = 554.2092.

2.2.1.27 *N*-(4-bromophenyl)-*N*-(2-(*tert*-butylamino)-1-(4-methoxyphenyl)-2-oxoethyl)-2-(3-oxo-3,4-dihydro-2*H*-benzo[*b*][1,4]-thiazin-2-yl)-acetamide (8iC)

The reaction was carried out as mentioned for the synthesis of 8. The desired compound was obtained as a pale yellow solid in 58% yield (155 mg), $R_f = 0.3$ (hexane:EtOAc, 7:3); $^1\text{H NMR}$ (400 MHz, CDCl_3): δ 8.52 (s, 1H), 7.25 (d, $J = 1.4$ Hz, 1H), 7.24 (d, $J = 1.3$ Hz, 1H), 7.12 (td, $J_1 = 7.7$ Hz, $J_2 = 1.4$ Hz, 1H), 7.05–6.93 (m, 4H), 6.82–6.76 (m, 1H), 6.71–6.67 (m, 2H), 5.94 (s, 1H), 5.78 (s, 1H), 5.28 (s, 2H), 4.13 (dd, $J_1 = 7.9$ Hz, $J_2 = 6.3$ Hz, 1H), 3.73 (s, 3H), 2.73 (dd, $J_1 = 16.2$ Hz, $J_2 = 6.3$ Hz, 1H), 2.22 (dd, $J_1 = 16.2$ Hz, $J_2 = 7.9$ Hz, 1H), and 1.31 (s, 9H); $^{13}\text{C NMR}$ (100 MHz, CDCl_3): δ 169.5, 168.7, 167.2, 159.5, 138.3, 135.8, 132.1, 131.6, 127.9, 127.3, 126.1, 123.8, 122.4, 119.5, 117.2, 113.8, 64.7, 55.2, 53.4, 51.6, 38.5, and 28.6; ES + HRMS calculated for $\text{C}_{29}\text{H}_{30}\text{BrN}_3\text{O}_4\text{SNa} = 620.1018$ and obtained = 620.1018.

2.2.1.28 *N*-(*tert*-butyl)-2-(*N*-(4-fluorophenyl)-2-(3-oxo-3,4-dihydro-2*H*-benzo[*b*][1,4]-thiazin-2-yl)-acetamido)-2-(4-methoxyphenyl)-acetamide (8iD)

The reaction was carried out as mentioned for the synthesis of 8. The desired compound was obtained as a pale brown solid in 55% yield (132 mg), $R_f = 0.3$ (hexane:EtOAc, 7:3); $^1\text{H NMR}$ (400 MHz, CDCl_3): δ 8.21 (s, 1H), 7.29–7.27 (m, 1H), 7.16–7.11 (m, 1H), 7.05–6.94 (m, 5H), 6.79 (d, $J = 8.0$ Hz, 1H), 6.69 (d, $J = 8.8$ Hz, 3H), 5.97 (s, 1H), 5.82 (s, 1H), 4.17–4.13 (m, 1H), 3.74 (s, 3H), 2.75 (dd, $J_1 = 16.2$ Hz, $J_2 = 6.3$ Hz, 1H), 2.24 (dd, $J_1 = 16.2$ Hz, $J_2 = 7.9$ Hz, 1H), and 1.33 (s, 9H); $^{13}\text{C NMR}$ (100 MHz, CDCl_3): δ 169.7, 168.8, 167.2, 160.7, 159.4, 135.8, 135.2, 132.2, 131.6, 12, 127.3, 126.3, 123.8, 119.6, 117.1, 113.7, 64.7, 55.2, 51.6, 38.5, 34, and 28.6; ES + HRMS calculated for $\text{C}_{29}\text{H}_{30}\text{FN}_3\text{O}_4\text{SNa} = 558.1839$ and obtained = 558.1840.

2.2.1.29 *N*-(*tert*-butyl)-2-(2-chlorophenyl)-2-(*N*-(3-chlorophenyl)-2-(3-oxo-3,4-dihydro-2*H*-benzo[*b*][1,4]-thiazin-2-yl)-acetamido)-acetamide (8jB)

The reaction was carried out as mentioned for the synthesis of 8. The desired compound was obtained as a white solid in 45% yield (112 mg), $R_f = 0.3$ (hexane:EtOAc, 7:3); $^1\text{H NMR}$ (400 MHz, CDCl_3): δ 9.12 (bs, 1H), 7.76–7.27 (m, 2H), 7.13–6.94 (m, 8H), 6.86–6.82 (m, 2H), 6.32 (s, 1H), 5.94 (bs, 1H), 4.17–4.12 (m, 1H), 2.81–2.70 (m, 1H), and 2.36–2.25 (m, 1H); $^{13}\text{C NMR}$ (100 MHz, CDCl_3): δ 169.5, 168.1, 167.6, 140.0, 135.9, 135.3, 131.4, 129.9, 129.4, 128.6, 127.9, 127.2, 126.7, 123.8, 119.8, 119.2, 117.3, 62.1, 51.9, 51.8, 38.4, and 28.7; ES + HRMS calculated for $\text{C}_{28}\text{H}_{27}\text{Cl}_2\text{N}_3\text{O}_3\text{SNa} = 578.1048$ and obtained = 578.1039.

2.2.1.30 *N*-(*tert*-butyl)-2-(*N*-(4-methoxyphenyl)-2-(3-oxo-3,4-dihydro-2*H*-benzo[*b*][1,4]-thiazin-2-yl)-acetamido)-butanamide (8kG)

The reaction was carried out as mentioned for the synthesis of 8. The desired compound was obtained as a pale brown solid in 52% yield (109 mg), $R_f = 0.35$ (hexane:EtOAc, 7:3); $^1\text{H NMR}$ (400 MHz, CDCl_3): δ 8.34 (bs, 1H), 7.30–7.28 (m, 1H), 7.21–7.14 (m, 2H), 7.06–6.99 (m, 1H), 6.90–6.79 (m, 4H), 6.55 (bs, 1H), 4.90–4.87 (m, 1H), 4.14–4.10 (m, 1H), 3.78 (s, 3H), 2.63 (dd, $J_1 = 16.0$ Hz, $J_2 = 7.2$ Hz, 1H), 2.33 (dd, $J_1 = 16.0$ Hz, $J_2 = 7.2$ Hz, 1H), 1.84–1.6 (m, 2H), 1.37 (s, 9H), and 0.89 (t, $J = 7.2$ Hz, 3H); $^{13}\text{C NMR}$ (100 MHz,

CDCl_3): δ 170.8, 169.6, 167.2, 159.4, 135.9, 130.7, 127.9, 127.3, 123.8, 119.8, 117.1, 114.5, 60.8, 55.4, 51.2, 38.4, 33.8, 28.6, 21.5, and 10.8; ES + HRMS calculated for $\text{C}_{25}\text{H}_{31}\text{N}_3\text{O}_4\text{SNa} = 492.1933$ and obtained = 492.1938.

2.3 Computational studies

2.3.1 Molecular modeling studies

In this study, we designed and synthesized novel 1,4-benzothiazine-based bisamides that might act as peptide deformylase inhibitors. After the pre-treatment of the peptide deformylase enzyme (PDB ID: 1Q1Y), the structure was corrected and completed. The natural product actinonin was used as the reference standard and was fully displayed. According to the docking score and drug-likeness, 28 candidate molecules were selected, and all of them could bind to the active site.

2.3.2 Protein preparation

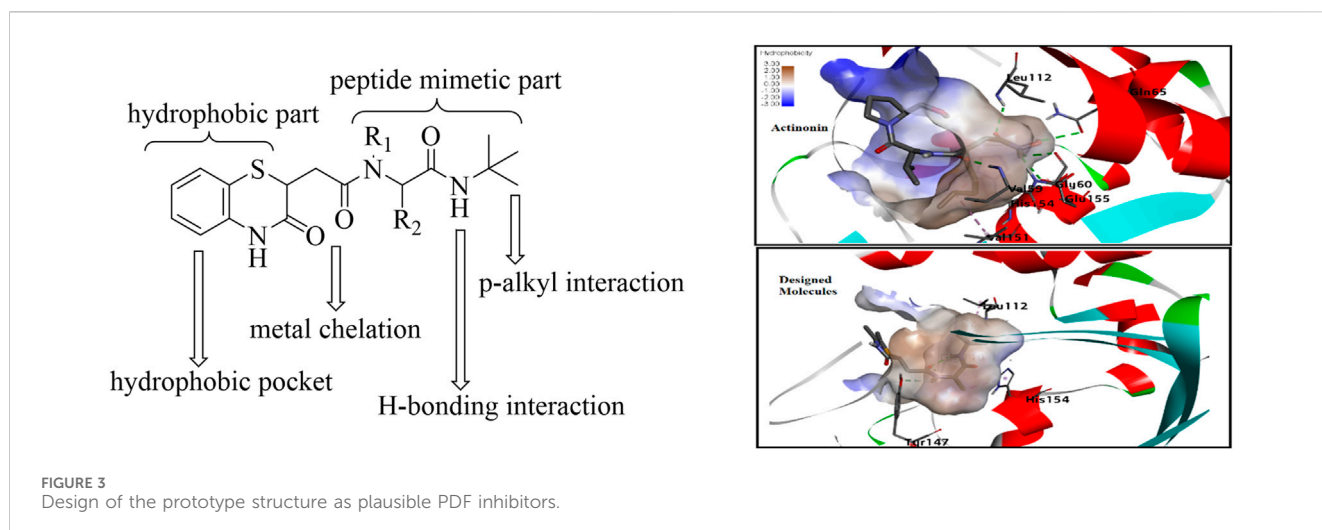
The X-ray crystallographic structure of the PDF protein was procured from the Research Collaboratory of Structural Bioinformatics (RCSB) Protein Data Bank (<http://www.rcsb.org>) (PDB ID: 1Q1Y), having a resolution of 1.90 Å (Yoon et al., 2004). MGLTools 1.5.6 (Molecular Graphics Laboratory, The Scripps Research Institute, La Jolla, United States) was used to model the protein. Energy minimization was performed using Swiss-PdbViewer (SPDBV 4.1.0, Swiss Institute of Bioinformatics). To remove the interference from water molecules, the protein molecule was desolvated. To free up the binding cavity, extra chains were cut out, and the co-crystal ligand was removed. After attaching polar hydrogens and assigning bond order, Gasteiger partial atomic charges were applied. The protein PDB format was changed to PDBQT by adding charges (Q) and switching the compatibility to AutoDock4 (T) type.

2.3.3 Ligand preparation

All the ligands were sketched using ChemDraw 15.0, subjected to energy minimization using the MM2 minimization protocol, and saved in PDB format. MGLTools version 1.5.6 was used for ligand modeling. The ligands were subjected to the software program, and the torsional degrees of freedom (torsdof) were added to each molecule. The Gasteiger–Marsili approach was then used to add partial atomic charges (Q) and make AutoDock4 (T) compatible, transforming each ligand to the PDBQT format.

2.3.4 Molecular docking and analysis

Molecular docking studies were performed using AutoDock Vina (Trott and Olson, 2010). The active site domain was encircled by a grid box with a spacing of 1 Å and 24 × 24 × 24 dimensions in all directions for x, y, and z planes with the resolution set to −18.189, 142.096, and 39.78 at the x, y, and z centers, respectively. The compounds were compared to the standard actinonin molecule based on the binding energy (kcal/mol), and the highest actives were determined. Using PyMOL, the docked complex was retrieved and saved in PDB format. In order to analyze the docked complexes, BIOVIA Discovery Studio Visualizer version 20 was used. Prior to docking, the docking studies were



validated using AutoDock Vina. For this, the co-crystal ligand and actinonin were removed and then redocked again within the active site pocket of the PDF receptor. The root mean square deviation (RMSD) value between the redocked conformer and the initial X-ray crystallographic conformation of the co-crystal was found to be 0.048. Validation using AutoDock Vina showed no appreciable differences. The least binding energy and the ligand–receptor interactions were considered for the docking analysis.

2.3.5 Predicted pharmacokinetic properties

The pharmacokinetic properties of the synthesized benzothiazine-3-one derivatives were analyzed using SwissADME (<http://www.swissadme.ch/>) and toxicity prediction utilizing the ProTox-II server (https://tox-new.charite.de/protox_II/). The program calculated the results automatically after inserting the smiles of the compounds.

2.3.6 Molecular dynamics simulation

To determine the stability of the docked complex and the ligand–protein time of contacts and residence interaction percentage, the molecular dynamics (MD) simulation was performed for compound **8bE** bound with the PDF receptor using the GROMINGEN Machine for Chemical Simulations (GROMACS) (Van Der Spoel et al., 2005) 2021.2 package. Ligand and protein topologies were created using Discovery Studio software and submitted for final simulation using CHARMM36 force field parameters. The energy minimization parameters were set for 5,000 steps using the steepest descent method. The MD simulation was conducted for 100 ns with constant temperature “T” (300 K), volume “V,” number of atoms “N” (NVT), and pressure “P” (1.0 bar) (NPT) GROMACS equilibration parameters. The leap-frog MD integrator was used, with an estimated frame rate of 1,000 per simulation. MD trajectories were analyzed for the protein and ligand: root mean square deviation RMSD, root mean square fluctuation (RMSF), radius of gyration (Rg), protein–ligand hydrogen bonding (H-bonds), and solvent-accessible surface area (SASA) during a 100-ns timeframe.

2.4 Biological assay

2.4.1 Protocols for microbiological assay

The protocols used here are a step-by-step adjustment and follow the guidelines described by the Clinical and Laboratory Standards Institute (CLSI), United States.

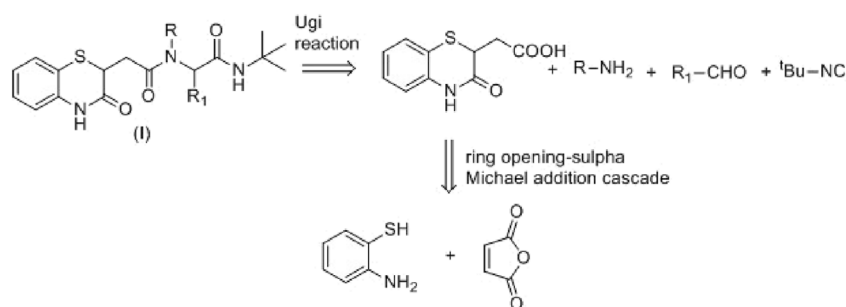
Media: The culture media were prepared using Luria-Bertani (LB) broth (Miller) without any supplements at a concentration of 25 g/L.

Bacteria: The assays were performed on MTCC 3160 *S. aureus*, which was cultured in LB broth 24 h before the experiment from a previously prepared bacterial colony plate. It was normalized to 0.08–0.13 OD₆₀₀ as a density equivalent to 10⁸ CFU/mL. This was used for inoculation.

Preparation of test molecules: All molecules were dissolved in DMSO to obtain a stock solution of 5 mg/mL. Before the experiment, aliquots of different concentrations were prepared by diluting the required quantity with dd water and then filtered via a 0.22- μ m filter. To avoid any effect of DMSO, its concentration was kept below 1% at each well.

2.4.2 Bacterial cell viability assay

Experimental procedure: All the experiments were done inside laminar air flow using pre-sterilized equipment like micropipettes, PBS solution, and LB medium microtiter plates. Here, 100 μ L of 1 mg/mL drug solution was added to 100 μ L of LB broth in the first column of a 48-well plate, and two-fold serial dilution was performed thereafter. Then, 100 μ L of bacterial suspension (10⁶ CFU/mL) was added to each well to obtain a final concentration of 5 \times 10⁵ CFU/mL. The well without drug was used as the positive control, the well with the media alone was used as the blank, and 10 μ g/mL amoxicillin was used as the negative control. The plate was incubated at 37°C for 16 h. The optical density of the bacterial cultures was measured at 600 nm using a Multiskan SkyHigh Microplate Spectrophotometer (Thermo Fisher Scientific). Data are presented as the mean standard deviation with n = 6 (Wiegand et al., 2008).



SCHEME 1
Retrosynthetic plan for the synthesis of the designed molecules.

2.4.3 MBIC determination by crystal violet assay

Experimental procedure: All the experiments were done inside laminar air flow using pre-sterilized equipment like micropipettes, PBS solution, and LB medium microtiter plates. In a pre-sterilized microtiter plate, 75 μ L of pre-sterilized Luria-Bertani broth (Miller) was added. To this, 20 μ L of previously prepared aliquots of the drug/molecule was added with vigorous pipetting to ensure complete solubilization. To this, 5 μ L of bacterial culture (OD = 0.01) was added, and the plate was incubated at 37°C for 16–18 h. The culture media were carefully pipetted and washed with 1 \times PBS (100 μ L \times 3). Then, 100 μ L solution of 4% paraformaldehyde was added to dd water and incubated for 30 min. Then, the solution was carefully removed and washed with 1 \times PBS (100 μ L \times 3). Then, 105 μ L of 0.1% crystal violet solution was added, incubated for 30 min, and then washed with 1 \times PBS (100 μ L \times 3). It was left to dry for 30 min, so no traces of the crystal violet solution were left. In most cases, a fine layer of a violet-colored film will be visible.

Then, 105 μ L ethanol was added and incubated for 10 min (a 33% solution of acetic acid in dd water can also be used, but it requires incubation of 30 min). Absorbance was read at 570 nm (O'Toole, 2011).

2.4.4 Catheter-associated biofilm formation

Experimental procedure: A natural rubber latex silicone catheter was used for this assay. The circular disks (0.2 cm height and 0.25 cm diameter) of the catheter were excised and kept in long-range (350 nm) UV radiation 12 h before the experiment. These were incubated in a 48-well microtiter plate along with the cultured *S. aureus* (0.01 OD₆₀₀) and test molecule for 24 h at 37°C under static conditions. After 24 h, crystal violet assay was used to quantify biofilm formation (Colomer-Winter et al., 2019).

3 Results and discussions

3.1 Design of molecules

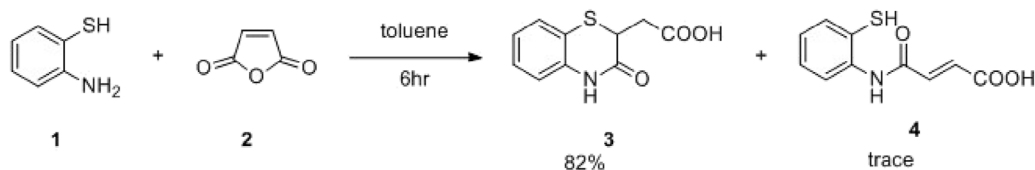
As supported by the molecular modeling data, the bisamide side chain could act as the therapeutically significant peptidomimetics part. The compound with prototype structure I was docked with the crystal structures of PDF from *S. aureus*, and the binding of the molecule was compared with the standard actinonin (Figure 3) (Yoon et al., 2004). The computational data showed that the

molecules could fit well within the binding pocket of the PDF receptor, and like the standard actinonin, the benzothiazine molecules would bind to the hydrophobic pocket of the receptor, in which the peptidomimetic part would be more adhered toward the pocket. The *tert*-butyl group could impart pi-alkyl interactions, and the -NH part of the amine could form a stable hydrogen bond with amino acid residues. In molecular modeling, another significant feature observed was the interaction with the Gly110 residues, and a literature report indicates that this interaction is essential for peptide deformylase (Kumar et al., 2014). Therefore, modifications only at R₁ and R₂ of the peptidomimetic part are planned with the hypothesis that it may provide better van der Waals interaction.

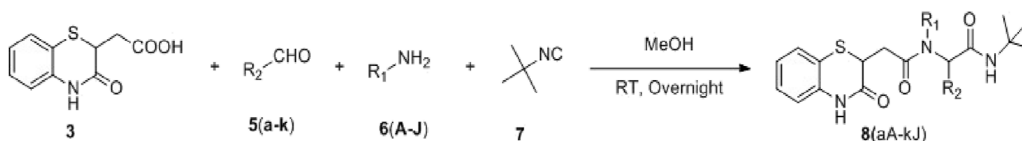
3.2 Synthesis

Maleic anhydride is a fascinating cyclic anhydride with vast applications in polymer science, biotechnology, or API synthesis (Kamada et al., 2003). In the presence of amines, maleic anhydride undergoes ring opening, followed by dehydrative cyclization to form *N*-substituted maleimides (Scheme 1) (Kaur et al., 2013). We recently demonstrated that the cyclization path of maleic anhydride can be controlled to produce benzoxazole derivatives (Kumar et al., 2023). Herein, we envisage that maleic anhydride in the presence of 2-aminothiophenol would undergo cascade anhydride ring opening, followed by intramolecular sulfa-Michael addition to produce the desired 1,4-benzothiazine-3-carboxylic acid derivative in one pot (Scheme 1), which could further be employed in the Ugi four-component reaction of 3 with a suitable amine, aldehyde, and isocyanide to achieve the designed molecule 8. The Ugi four-component reaction is one of the useful multicomponent reactions for synthesizing diverse heterocyclic scaffolds, natural products, and biologically active molecules (Fouad et al., 2020).

With that hypothesis, the reaction was carried out, and 1,4-benzothiazine-3-carboxylic acid was obtained in 82% yield along with 15% of the non-cyclized product. Then, to achieve better conversion, 1 equivalent of Et₃N was used, and within 3 h, the yield of the desired product improved significantly to 96% (Scheme 2), and no non-cyclized product was obtained. Then, as hypothesized, the Ugi reaction of 3 with *tert*-butyl isocyanide,



SCHEME 2
One-pot synthesis of 1,4-benzothiazine-3-carboxylic acid.



SCHEME 3
Synthesis of benzothiazine-3-one containing bisamide derivatives.

benzaldehyde, and benzyl amine in MeOH was carried out at room temperature. As aimed, within 14 h, the reaction was completed, and isolation of the compound afforded compound **8aA** in 60% yield (Scheme 3). Then, the reaction scope was explored by using different aldehydes and amines containing electron-donating and electron-withdrawing groups at the different positions of the aromatic ring (Table 1). The isocyanides were not changed as in molecular docking, the *tert*-butyl group exerts three pi-alkyl interactions, which is responsible for good docking scores. Aliphatic amines like tryptamine or benzyl amines were used to check the effect of the carbon chain on the activities.

3.3 Antibacterial screening

After the structural characterization by HRMS and NMR spectra, all the newly synthesized molecules were evaluated for *in vitro* antibacterial activity (Table 1) against both Gram-positive and Gram-negative bacteria, including *S. aureus* (MTCC 3160), *Bacillus cereus* (MTCC 1272), *Escherichia coli* (MTCC 1667), and *Vibrio cholerae*. Among the compounds screened, nine compounds exhibited very good antibacterial activities against *S. aureus*, of which compound **8bE** showed better activity than the references gentamicin and actinonin. In these compounds, it was observed that the substitution of aromatic rings at the *para* position leads to maximal efficacy. Of all the compounds tested, **8bE** showed the highest activity with an MIC₅₀ value of $6.16 \pm 2.17 \mu\text{g/mL}$ (Table 1, entry 9). It contained tryptamine as amine and 4-nitrobenzaldehyde as the aldehyde part. Furthermore, in most cases, alkyl-substituted anilines showed better inhibition except in the cases of 4-chlorobenzaldehyde (Table 1, entry 12). So, it can be assumed that alkyl amines are a better substrate in this case, along with the *para*-substituted benzaldehyde substrate. It is crucial to note that heteroaromatic rings, such as furfuryl, are also active (Table 1, entry 17 & 18), while aliphatic aldehydes do not show activity (Table 1, entry 28). Another important feature is that other

substitutions at *ortho* or *meta* in the benzaldehyde ring do not show potent activity, with only the *m*-methyl analog showing potential activity (Table 1, entries 19 and 20).

3.4 Biofilm inhibition screening

After checking the MIC values, the compounds were further screened against *S. aureus* biofilms. It was found that compounds **8bE** and **8cE**, which were the most potent molecules against *S. aureus*, also demonstrated excellent biofilm inhibitory activities (Table 2). This result indicated that compounds **8bE** and **8cE** can display dual inhibitory properties.

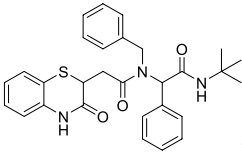
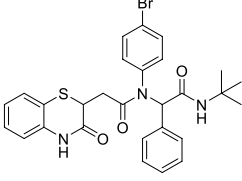
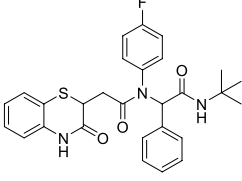
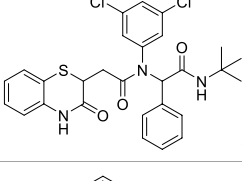
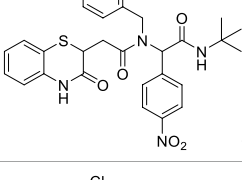
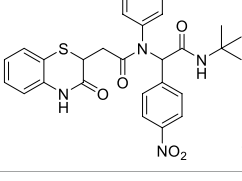
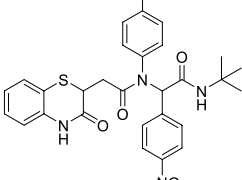
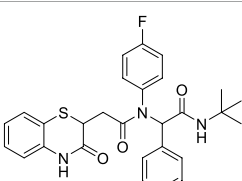
3.4.1 Validation of biofilm inhibitory properties

Furthermore, a field emission scanning electron microscope (SEM) was used to validate the anti-biofilm effect of **8bE**. A *S. aureus* biofilm developed on the surface of glass slides in a multi-well plate (Kong et al., 2018), and to this plate, compound **8bE** was incubated at concentrations of 6 $\mu\text{g/mL}$ and 12 $\mu\text{g/mL}$. The morphology of the untreated *S. aureus* biofilm is shown in Figures 4A,B. On incubation with 6 $\mu\text{g/mL}$ of **8bE**, disruption of the biofilm was visible (Figure 4C). On increasing the concentration to 12 $\mu\text{g/mL}$, patches of the remaining biofilm were visible (Figure 4D). On 1,000 \times magnification, the biofilm appeared as a monolayer with cells scattered throughout the layer (Figure 4E). On further magnification of 7,000 \times , bacterial cells appeared as finely dispersed with no visible sign of clumping (Figure 4F). The SEM pictures supported the ability of the molecule to inhibit biofilm formation.

3.4.2 Biofilm inhibitory assay on the urinary catheter

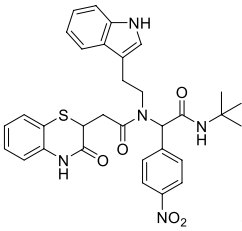
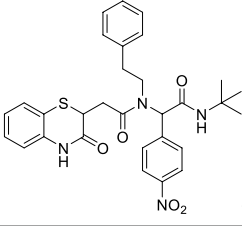
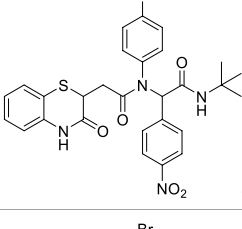
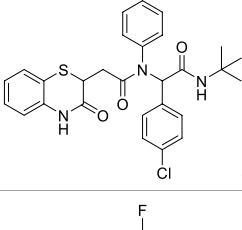
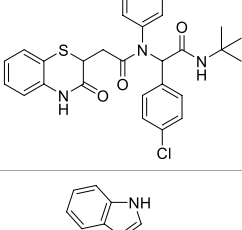
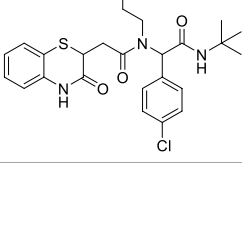
After confirming the biofilm inhibitory properties of **8bE**, we extended the scope of the study to controlling biofilm inhibition in medical devices like urinary catheters. The impact of catheter-

TABLE 1 Docking scores, yield, and antibacterial activities of the synthesized compounds.

Entry	Compound	Docking score	Yield (%)	Antibacterial activity MIC ($\mu\text{g/mL}$)			
				Sa	Bc	Ec	Vc
1	 8aC	-7.8	60	55-60	>100	>100	>100
2	 8aC	-8.0	54	55-60	>100	>100	>100
3	 8aD	-8.2	51	55-60	>100	>100	>100
4	 8aJ	-8.6	65	55-60	>100	>100	>100
5	 8bA	-8.7	60	50.48 ± 1.28	>100	>100	>100
6	 8bB	-9.1	55	30.48 ± 1.55	>100	>100	>100
7	 8bC	-8.5	58	47.5 ± 2.5	>100	>100	>100
8	 8bD	-8.6	56	46.25 ± 2.25	>100	>100	>100

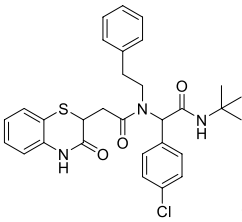
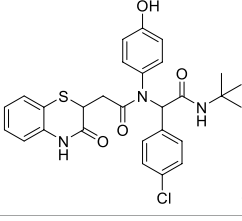
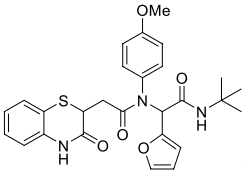
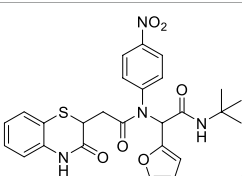
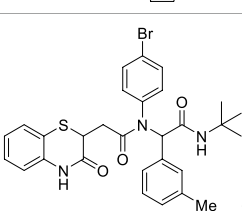
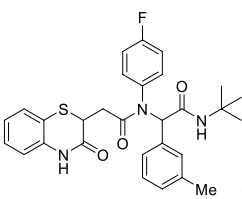
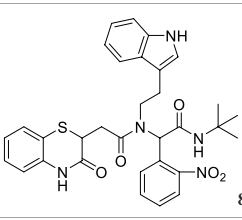
(Continued on following page)

TABLE 1 (Continued) Docking scores, yield, and antibacterial activities of the synthesized compounds.

Entry	Compound	Docking score	Yield (%)	Antibacterial activity MIC ($\mu\text{g/mL}$)			
				Sa	Bc	Ec	Vc
9	 8bE	-8.3	64	6.16 \pm 2.17	>100	>100	>100
10	 8bF	-7.0	60	34.15 \pm 2.42	>100	>100	>100
11	 8bI	-8.4	51	42.62 \pm 3.45	>100	>100	>100
12	 8cC	-7.9	52	15.56 \pm 1.44	>100	>100	>100
13	 8cD	-8.4	51	25.55 \pm 2.45	>100	>100	>100
14	 8cE	-9.0	52	12.39 \pm 1.64	>100	>100	>100

(Continued on following page)

TABLE 1 (Continued) Docking scores, yield, and antibacterial activities of the synthesized compounds.

Entry	Compound	Docking score	Yield (%)	Antibacterial activity MIC ($\mu\text{g/mL}$)			
				Sa	Bc	Ec	Vc
15	 8cF	-8.1	55	38.47 ± 1.14	>100	>100	>100
16	 8cI	-7.8	55	48.47 ± 2.13	>100	>100	>100
17	 8dG	-7.7	48	28.36 ± 3.24	>100	>100	>100
18	 8dH	-8.0	48	18.47 ± 1.28	>100	>100	>100
19	 8cC	-8.3	52	22.45 ± 0.85	>100	>100	>100
20	 8eD	-7.5	55	47.62 ± 1.75	>100	>100	>100
21	 8fE	-7.5	59	>100	>100	>100	>100

(Continued on following page)

TABLE 1 (Continued) Docking scores, yield, and antibacterial activities of the synthesized compounds.

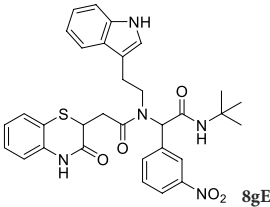
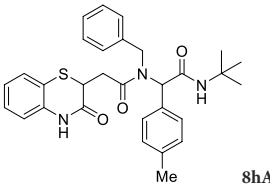
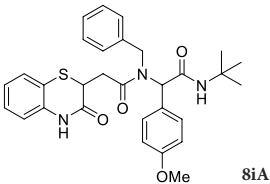
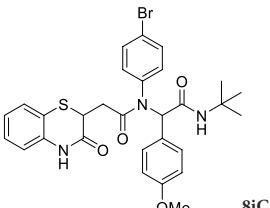
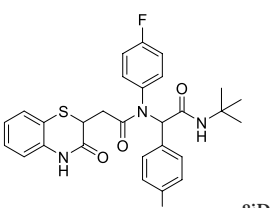
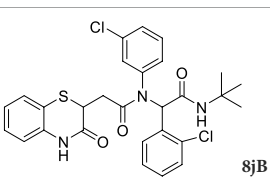
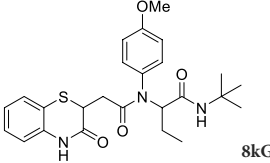
Entry	Compound	Docking score	Yield (%)	Antibacterial activity MIC ($\mu\text{g/mL}$)			
				Sa	Bc	Ec	Vc
22	 8gE	-8.4	55	>100	>100	>100	>100
23	 8hA	-8.1	65	55-60	>100	>100	>100
24	 8iA	-7.7	62	55-60	>100	>100	>100
25	 8iC	-7.3	58	55-60	>100	>100	>100
26	 8iD	-7.4	55	55-60	>100	>100	>100
27	 8jB	-7.4	45	>100	>100	>100	>100
28	 8kG	-7.3	52	>100	>100	>100	>100
29 (Margolis et al., 2000; Clements et al., 2001; Jung et al., 2016)	Actinonin	-7.1		16	0.192	64	-
30 (Scazzocchio et al., 2006; Coutinho et al., 2010; Bier et al., 2015)	Gentamicin	-7.3		12.5	4	4	2

TABLE 2 Biofilm inhibitory activities of the synthesized compounds.

Entry	Compound	MBIC (µg/mL)	Entry	Compound	MBIC (µg/mL)	Entry	Compound	MBIC (µg/mL)
1	8aA	80	11	8bI	80	21	8fE	>100
2	8aC	80	12	8cC	34.26 ± 1.74	22	8gE	>100
3	8aD	80	13	8cD	80	23	8hA	80
4	8aJ	80	14	8cE	14.31 ± 2.44	24	8iA	80
5	8bA	80	15	8cF	42.16 ± 1.86	25	8iB	80
6	8bB	80	16	8cI	80	26	8iD	80
7	8bC	50–55	17	8dG	36.49 ± 1.87	27	8jB	>100
8	8bD	50–55	18	8dH	24.32 ± 2.54	28	8kG	>100
9	8bE	10.42 ± 2.18	19	8eC	45 ± 1.07	29 (Al-Musawi et al., 2020)	Trans-chalcone	20
10	8bF	45.36 ± 3.24	20	8eD	80	30 (Park et al., 2022)	Kanamycin	50

The bold value highlights the highest MBIC values obtained by prepared derivatives.

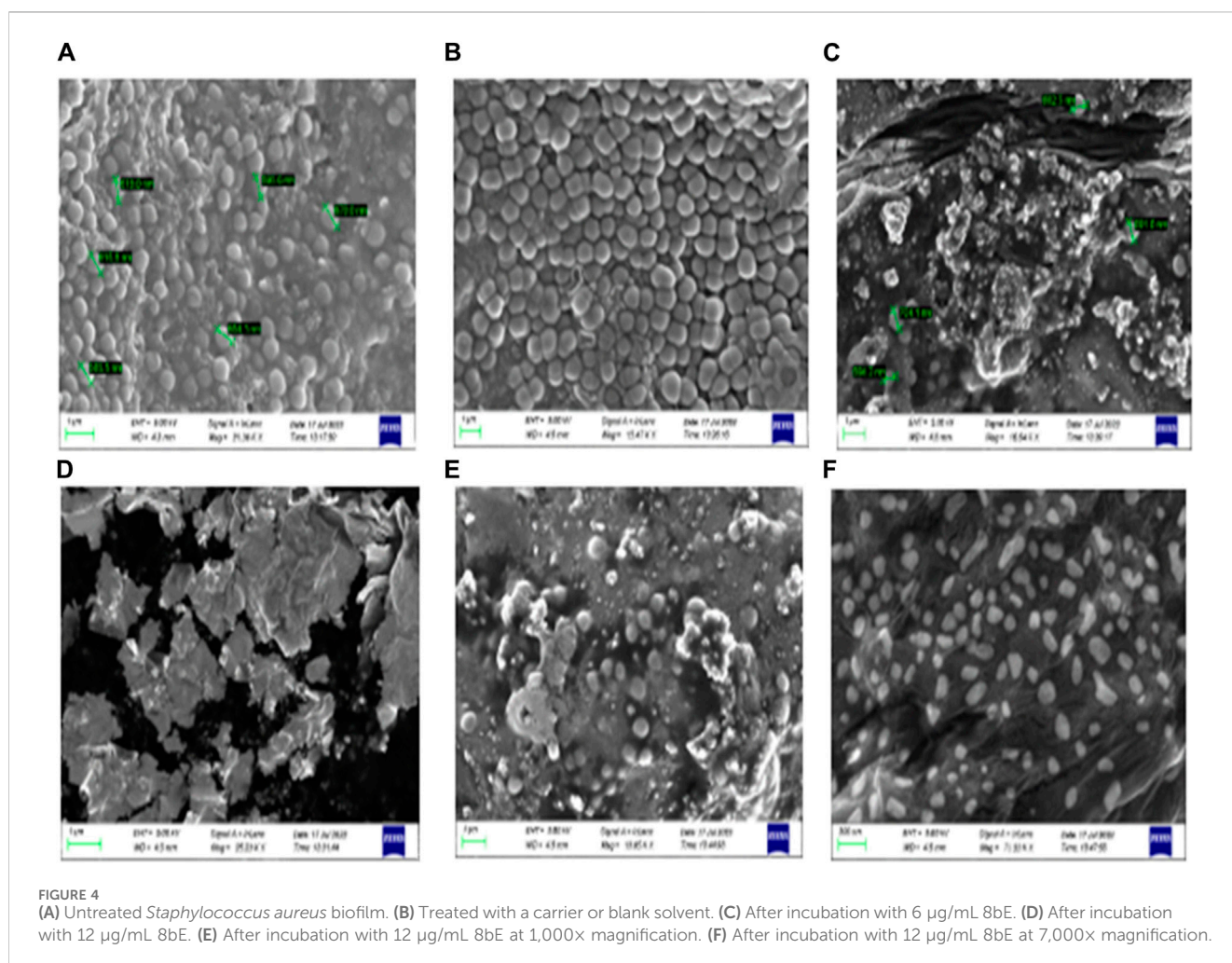


FIGURE 4 (A) Untreated *Staphylococcus aureus* biofilm. (B) Treated with a carrier or blank solvent. (C) After incubation with 6 µg/mL 8bE. (D) After incubation with 12 µg/mL 8bE. (E) After incubation with 12 µg/mL 8bE at 1,000x magnification. (F) After incubation with 12 µg/mL 8bE at 7,000x magnification.

associated infections on hospitalized patients is enormous. As per the CDC, approximately 75% of UTIs for hospitalized patients are associated with catheter and catheter-related bloodstream infection

(CRBSI), which causes about 18.2% mortality each year (Zhong et al., 2021). Therefore, developing a molecule that can control the biofilm formation on urinary catheters is urgently needed. Here, we

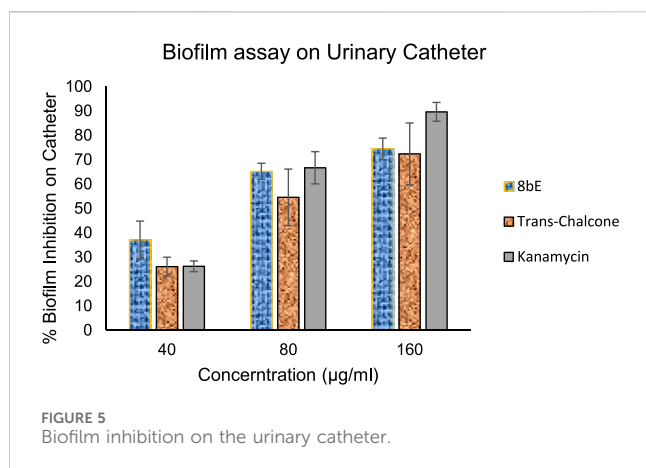


FIGURE 5
Biofilm inhibition on the urinary catheter.

checked the effect of our lead molecule, **8bE**, on biofilm formation associated with viable but non-culturable (VBNC) *S. aureus* on urinary catheters (Figure 5) (Colomer-Winter et al., 2019). For this purpose, we opted to observe biofilm formation in the presence of our lead molecule, **8bE**, at different concentrations and compare it with the antibacterial drug molecule kanamycin and non-specific moiety trans-chalcone.

At higher concentrations (160 µg/mL), kanamycin shows excellent inhibition of biofilm formation, which can be attributed to its potent antibacterial activity. However, as the concentration is decreased to 40 µg/mL, the effect is reduced to ~25%, whereas synthesized molecule **8bE** shows around 37% inhibition at this concentration, outperforming the reference standard kanamycin or trans-chalcone. This indicates the remarkable application of **8bE** against VBNC species.

3.5 Molecular docking studies

We then attempted to find the interactions responsible for the activity of compounds. Among the actives, one is compound **8bE** (p-nitrophenyl substituent), which is highlighted here (Figure 6).

Compound **8bE** has a binding energy of -8.3 kcal/mol, whereas the standard actinonin has a binding energy of -7.1 kcal/mol. It offers a strong hydrogen bond between one of the carbonyl oxygen atoms with $-NH$ of Val:59, with a distance of 2.93 Å. One more hydrogen bond was observed between the carbonyl oxygen of the benzothiazine moiety with the $-NH$ of Asn:117, having a distance of 2.27 Å. Another H-bond was observed between $-N$ and O of the nitro with $-NH$ of Gln:65, with a distance of 2.37 Å. The last H-bond had a distance of 1.87 Å between $-NH$ of indole and the hydroxyl "O" of Tyr:147. Apart from van der Waals interaction, three pi-alkyl interactions were noted between the compound and Val:151, Leu:105, and Leu:112, respectively. One pi-pi T-shaped interaction was observed between the compound and the His:154 residue. A pi-cation interaction was also observed with the Arg:56 residue and two weak C-H bond interactions with amino acid residues Val:59 and Glu:185, respectively. The standard molecule, actinonin, shows five hydrogen bonds and two pi-alkyl interactions. All the molecules showed better docking interactions than the standard.

Figure 6 highlights the 2D and 3D interaction images of compound **8bE** against *S. aureus* PDF. **8fE** (o-nitrophenyl substituent) has a low docking score of -7.5 kcal/mol. It shows a total of three hydrogen bonding interactions: one with $-NH$ of Gly:110 and carbonyl oxygen of the molecule (2.90 Å), one with $-C=O$ of Gly:110 and $-NH$ of the benzothiazine part of the molecule (2.07 Å), and an H-bond with $-N=O$ of the nitro and $-NH$ of Arg:56 (2.23 Å). Other than van der Waals interaction, one pi-sigma interaction with Val:59; one pi-anion interaction with Glu:155; three pi-alkyl interactions with Val:59, Pro:78, and Leu:112; one pi-sulfur interaction with the modified cysteine residue Csd:111; and one weak carbon-hydrogen bond with Gly:110 were observed. Compound **8gE** (m-nitrophenyl substituent) has a comparable docking score of -8.4 kcal/mol. It showed two H-bonds with $-N=O$ of nitro and $-NH$ of both Val:59 (2.29 Å) and Gly:60 (2.32 Å). One H-bond with $-NH$ of indole of the compound and hydroxyl-O- of Tyr:147 (1.77 Å); two H-bonds between $C=O$ of benzothiazine of the compound and $-NH$ of both Arg:56 (2.04 Å) and Asn:117 (2.91 Å); one pi-pi T-shaped interaction between the compound and His:154; four pi-alkyl/alkyl interactions with Leu:112, Val:59, Val:151, and Arg:56; and two weak carbon-hydrogen bonds with Gly:110 and Glu:185 were also observed. Compared to the

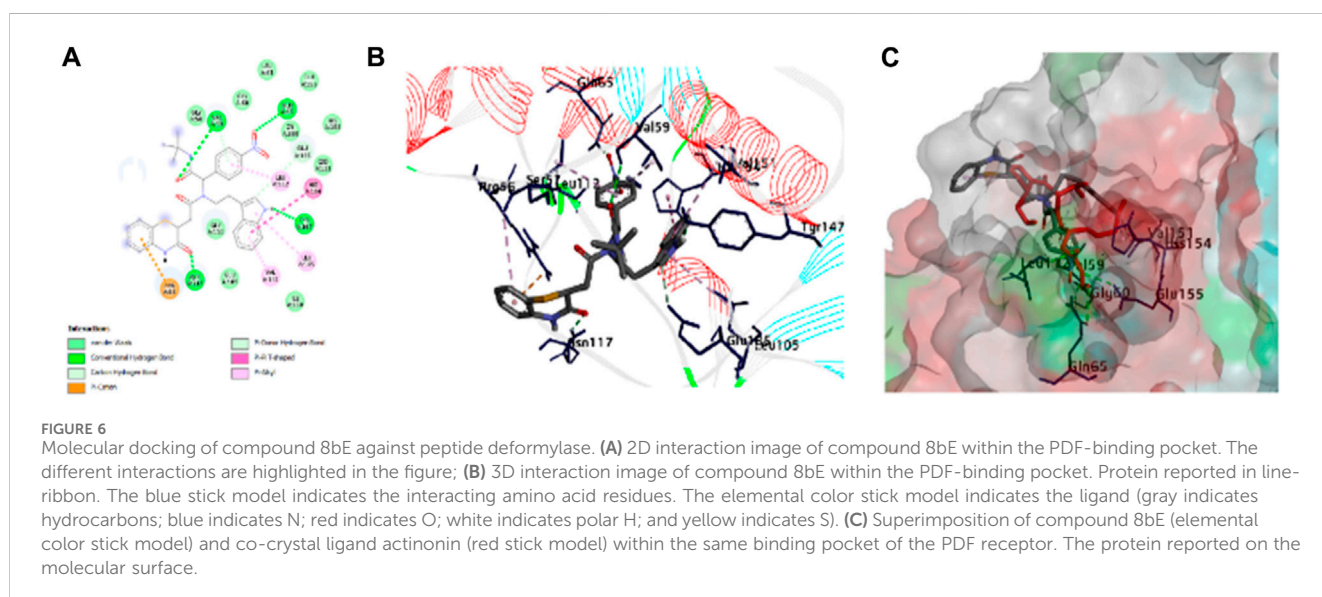


TABLE 3 Pharmacokinetics and toxicity profiling data.

S. No	Property	Actinonin	8bE	8cE
1	Log S (Aq solubility)	-2.28 (soluble)	-6.16 (poorly soluble)	-6.69 (poorly soluble)
2	Log Kp (skin permeability) cm/s	-7.55	-6.54	-5.90
3	BBB permeation	No	No	No
4	GI absorption	High	Low	Low
5	Bioavailability score	0.55	0.55	0.55
6	P-gp substrate	Yes	Yes	Yes
7	CYP1A2 inhibitor	No	No	Yes
8	CYP2C19 inhibitor	No	Yes	Yes
9	CYP2C9 inhibitor	No	Yes	Yes
10	CYP2D6 inhibitor	No	No	Yes
11	CYP3A4 inhibitor	No	Yes	Yes
12	Toxicity class	4	4	4
13	Hepatotoxicity	Inactive	Inactive	Inactive
14	Carcinogenicity	Active	Active	Inactive
15	Mutagenicity	Inactive	Active	Inactive
16	Cytotoxicity	Inactive	Inactive	Inactive

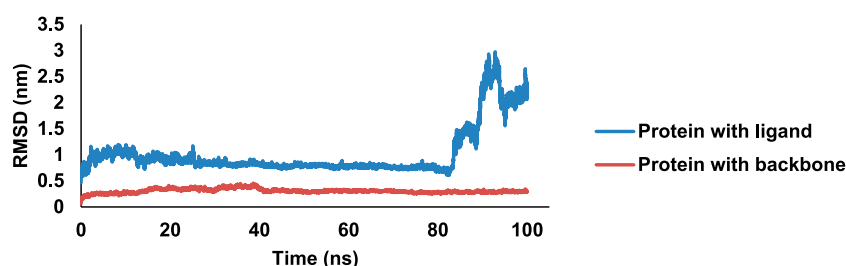


FIGURE 7 MD simulation data on the 8bE complex in 100-ns runtime; RMSD curve of the complex and protein.

interactions of actinonin, only three interacting amino acid residues were found similar with 8fE interactions, and all were weak interactions. With both 8bE and 8gE, five interactions were similar to actinonin, among which, in both cases, two were strong H-bonds. Detailed molecular modeling with other derivatives is provided in [Supplementary Table S1](#) and [Supplementary Figures S57 and S58](#). We observed that even small changes in the ligand molecule resulted in variations in the docking score. Upon comparing these docking results with the antimicrobial activity, we concluded that the molecules exhibiting strong activity (8bE and 8cE) both interacted with Tyr:147 and His:154. These specific amino acids are part of the catalytic triad responsible for the deformylation process and are conserved across different organisms. It is noteworthy that in other organisms, Tyr:147 is substituted with Leu or Gly. This suggests that the synthesized molecules might have specificity toward Sa-PDF. Additionally, the authors of PDB ID: 1Q1Y noted that during attempts to crystallize, Cys:111 was oxidized to cysteine sulfonic acid (Cys-SO₃H), mentioned

as Csd:111 ([Yoon et al., 2004](#)). We observed that many of our molecules with high docking scores formed conventional hydrogen bonds with this modified amino acid. Providing strong interactions with catalytic triad amino acids and reducing off-targeting interactions may show better activity and a good docking score. Some molecules like 8bB, although having interactions with the catalytic triad, have more off-targeting interactions, thus leading to poor activity. We believe it is better to target the catalytic domains of target enzymes to improve the efficacy of lead molecules.

3.6 *In silico* prediction of pharmacokinetic and toxicity profiles

The pharmacokinetic properties of the molecules were predicted using the SwissADME web server ([Daina et al., 2017](#)), and the toxicity analysis was performed using the ProTox-II web server ([Banerjee](#)

et al., 2018). The results indicated that actinonin is aqueous soluble (Log S = -2.28) with high gastrointestinal absorption, whereas compounds **8bE** (Log S = -6.16) and **8cE** (Log S = -6.69) are poorly soluble with low gastrointestinal (GI) absorption. The skin permeability value (log kp in cm/s) for actinonin is -7.55, and for **8bE** and **8cE**, they are -6.54 and -5.90, respectively. The lower the skin permeability value, the lesser the skin permeability; hence, **8bE** and **8cE** have better skin permeability than actinonin. None of the molecules can penetrate the blood-brain barrier (BBB) similar to actinonin, thereby reducing the neurotoxicity, and thus, P-glycoprotein (P-gp) substrates (efflux pumps that protect the CNS from harmful xenobiotics) are safer molecules. Cytochrome P450 isoenzymes are important enzymes for drug metabolism, the inhibition of which may lead to drug accumulation in the body, causing adverse reactions (Das et al., 2023). Although actinonin does not inhibit any cytochrome isoenzymes, compound **8bE** shows inhibition for CYP2C19, CYP2C9, and CYP3A4 while not against CYP1A2 and CYP2D6, and compound **8cE** inhibits all the cytochromes. All three have the same bioavailability score of 0.55. **8bE** and **8cE** fall under the type IV class of toxicity (2,000 < LD₅₀ ≤ 5,000 mg/kg body weight), as per a globally harmonized system of classification of labeling of chemicals (OSHA, <https://www.osha.gov/hazcom>), similar to actinonin. Actinonin is non-hepatotoxic, non-mutagenic, and non-cytotoxic but active in carcinogenicity. **8bE** is active in carcinogenicity and mutagenicity but non-hepatotoxic and non-cytotoxic. **8cE** is non-hepatotoxic, non-mutagenic, non-carcinogenic, and also non-cytotoxic. Table 3 shows the properties in detail.

3.7 Molecular dynamics simulation data

One of the most active compounds, **8bE**, in complex with PDF was then subjected to MD simulations to determine the stability of the complex in a 100-ns MD runtime. RMSD is a measure of the protein-ligand complex stability. It determines the equilibration period of the MD runtime and denotes the dynamical behavior of both the protein and the ligand in the isobaric-isothermal simulation period (Sargsyan et al., 2017). The free protein with respect to the backbone has minimal deflections along the RMSD trajectory, initiating from 0.1 nm, having an average of approximately 0.3 nm, with an almost stable curve, throughout the 100-ns run. When the protein is in complex with ligand **8bE**, the RMSD curve drifts higher compared to the free protein, starting from 0.5 nm, indicating slightly more deviations. Initial instability was observed up to 27 ns; later, the curve stabilized rapidly with minimal or no deflections up to 83 ns (Figure 7). After 83 ns, large deflections and wobbles occur, determining the instability of the complex, with an RMSD increase to 2.5 nm after 90 ns. RMSF refers to the fluctuations or local changes that occur when a ligand is attached to a protein during the isobaric-isothermal MD runtime. More residue fluctuations can lead to poor ligand-protein binding and dissociation from the binding pocket during the MD runtime (Joshi et al., 2021). The protein-ligand complex has a lower RMSF value of 0.15 nm and reaches up to 0.7 nm. The RMSF curve represents a stable curve with minimal fluctuations up to residue number 1,050. A slight fluctuation occurs at around 1,220–1,386 residues and then stabilizes up to 2,500. Then, the

RMSF curve shows major fluctuations. Overall, the RMSF curve stabilizes approximately at an average of 0.17 nm, indicating that ligand-protein binding is stable with minimal deflections. Rg assesses the structural compactness of the protein-ligand complex and decides whether the protein is stable or unstable based on fluctuation ranges during MD runtime. Rg values should not exhibit significant fluctuations during the MD run duration (Shahbaaz et al., 2019). The Rg curve is highly stable throughout the 100-ns runtime, having an average value of 1.7 nm. Hydrogen bonding (H-bonds) is the strongest bond involved in protein-ligand interaction, and it predicts the complex's stability. The MD simulation relies heavily on hydrogen bonding. Greater the H-bonds, higher the stability of the complex throughout the MD runtime and *vice versa* (Das et al., 2023). During the 100-ns run, a maximum of 8 H-bonds were achieved within the 4-ns runtime. However, the complex stabilized and had a minimum of three H-bonds in average throughout the 100-ns runtime. After docking studies, four H-bonds were observed, and after MD simulation, three H-bonds were observed in average throughout the runtime, thus indicating a stable complex. The SASA is an important parameter of MD simulation study, which determines the surface of the protein accessible to solvent molecules when it forms a strong binding with the ligand and can thus predict the flexibility and important conformational changes occurring during the protein-ligand interaction (Marsh and Teichmann, 2011). The complex has a SASA range of an area of 102–116 nm², with an average of 110 nm². No major deflections were observed throughout the MD runtime; thus, the complex was bonded strongly (Supplementary Figures S59–S63).

4 Conclusion

In conclusion, based on computational design, we discovered a new series of (1,4)-benzothiazine-3-one containing bisamide derivatives as antibacterial and antibiofilm agents against *S. aureus*. Molecular modeling against peptide deformylase of *S. aureus* showed the important interactions of the molecule responsible for its activity. Furthermore, the application of these molecules is demonstrated in controlling the biofilm formation on urinary catheters. Further work to expand the scope of SAR (Structure Activity Relationship), toxicity, and *in vivo* applications is in progress, which will be explained soon.

Data availability statement

The original contributions presented in the study are included in the article/Supplementary Material; further inquiries can be directed to the corresponding author.

Author contributions

KN: writing-original draft, visualization, validation, supervision, software, methodology, investigation, formal analysis, data curation, and conceptualization. AD: writing-review and editing, visualization, validation, software, methodology, investigation, formal analysis, and data curation. MU: writing-review and editing, visualization,

methodology, investigation, and formal analysis. SN: writing–review and editing, visualization, validation, methodology, investigation, formal analysis, and data curation. RB: writing–review and editing, visualization, validation, methodology, investigation, formal analysis, and data curation. AK: writing–review and editing, visualization, methodology, investigation, formal analysis, and data curation. KA: writing–review and editing, visualization, validation, methodology, investigation, and formal Analysis. UM: writing–review and editing, visualization, validation, supervision, resources, project administration, funding acquisition, formal analysis, and conceptualization. SB: writing–review and editing, writing–original draft, supervision, resources, project administration, funding acquisition, formal analysis, and conceptualization.

Funding

The author(s) declare that financial support was received for the research, authorship, and/or publication of this article. This study was supported by the NIPER-Kolkata AMR research fund from the Department of Pharmaceuticals, Ministry of Chemicals and Fertilizers, Government of India.

Acknowledgments

The authors acknowledge the Department of Pharmaceuticals, Ministry of Chemicals and Fertilizers, Government of India, for

References

- Ahmad, M., Aslam, S., Bukhari, M. H., Montero, C., Detorio, M., Parvez, M., et al. (2014). Synthesis of novel pyrazolobenzothiazine 5, 5-dioxide derivatives as potent anti-HIV-1 agents. *Med. Chem. Res.* 23, 1309–1319. doi:10.1007/s00044-013-0718-x
- Al-Musawi, E. T., Aljabori, K. M., and Al-Mathkhury, H. J. (2020). Effect of chalcone on the formation of biofilms and expression of virulence genes in methicillin-resistant staphylococcus aureus. *Biochem. Cell. Arch.* 20 (1). doi:10.35124/bca.2020.20.1.1797
- Aubart, K., and Zalacain, M., (2006). Peptide deformylase inhibitors. *Prog. Med. Chem.* 44, 109–143. doi:10.1016/s0079-6468(05)44403-3
- Badshah, S. L., and Naeem, A. (2016). Bioactive thiazine and benzothiazine derivatives: green synthesis methods and their medicinal importance. *Molecules* 21 (8), 1054. doi:10.3390/molecules21081054
- Banerjee, P., Eckert, A. O., Schrey, A. K., and Preissner, R. (2018). ProTox-II: a webserver for the prediction of toxicity of chemicals. *Nucleic. acids. Res.* 46 (W1), W257–W263. doi:10.1093/nar/gky318
- Belete, T. M. (2019). Novel targets to develop new antibacterial agents and novel alternatives to antibacterial agents. *Hum. Microbiome. J.* 11, 100052. doi:10.1016/j.humic.2019.01.001
- Bier, N., Schwartz, K., Guerra, B., and Strauch, E. (2015). Survey on antimicrobial resistance patterns in *Vibrio vulnificus* and *Vibrio cholerae* non-O1/non-O139 in Germany reveals carbapenemase-producing *Vibrio cholerae* in coastal waters. *Front. Microb.* 6, 1179. doi:10.3389/fmicb.2015.01179
- Clements, J. M., Beckett, R. P., Brown, A., Catlin, G., Lobell, M., Palan, S., et al. (2001). Antibiotic activity and characterization of BB-3497, a novel peptide deformylase inhibitor. *Antimicrob. Agents. Chemother.* 45 (2), 563–570. doi:10.1128/aac.45.2.563-570.2001
- Colomer-Winter, C., Lemos, J. A., and Flores-Mireles, A. L. (2019). Biofilm assays on fibrinogen-coated silicone catheters and 96-well polystyrene plates. *Bio-protocol* 9 (6), e3196. doi:10.21769/BioProtoc.3196
- Coutinho, H. D., Costa, J. G., Lima, E. O., Falcao-Silva, V. S., and Siqueira-Júnior, J. P. (2010). Increasing of the aminoglycoside antibiotic activity against a multidrug-resistant *E. coli* by *Turnera ulmifolia* L. and chlorpromazine. *Bio. Res. Nur.* 11 (4), 332–335. doi:10.1177/1099800409340052
- Daina, A., Michielin, O., and Zoete, V. (2017). SwissADME: a free web tool to evaluate pharmacokinetics, drug-likeness and medicinal chemistry friendliness of small molecules. *Sci. Rep.* 7 (1), 42717. doi:10.1038/srep42717
- financial support. The authors thank Pallab Dutta and Dipanjan Ghosh, NIPER-Kolkata, for their help in the SEM and antibacterial studies. The authors also acknowledge the LC-MS facility, NIPER-Kolkata, for the mass data.

Conflict of interest

The authors declare that the research was conducted in the absence of any commercial or financial relationships that could be construed as a potential conflict of interest.

Publisher's note

All claims expressed in this article are solely those of the authors and do not necessarily represent those of their affiliated organizations, or those of the publisher, the editors, and the reviewers. Any product that may be evaluated in this article, or claim that may be made by its manufacturer, is not guaranteed or endorsed by the publisher.

Supplementary material

The Supplementary Material for this article can be found online at: <https://www.frontiersin.org/articles/10.3389/fchem.2024.1420593/full#supplementary-material>

Das, A., Matada, G. S. P., Dhiwar, P. S., Raghavendra, N. M., Abbas, N., et al. (2023). Molecular recognition of some novel mTOR kinase inhibitors to develop anticancer leads by drug-likeness, molecular docking and molecular dynamics based virtual screening strategy. *Comput. Tox.* 25, 100257. doi:10.1016/j.comtox.2022.100257

de Oliveira, A., Pinheiro-Hubinger, L., Pereira, V. C., Riboli, D. F. M., Martins, K. B., Romero, L. C., et al. (2021). Staphylococcal biofilm on the surface of catheters: electron microscopy evaluation of the inhibition of biofilm growth by RNAIII inhibiting peptide. *Antibiotics* 10 (7), 879. doi:10.3390/antibiotics10070879

Foster, T. J., Geoghegan, J. A., Ganesh, V. K., and Höök, M. (2014). Adhesion, invasion and evasion: the many functions of the surface proteins of *Staphylococcus aureus*. *Nat. Rev. Microbiol.* 12 (1), 49–62. doi:10.1038/nrmicro3161

Fouad, M. A., Abdel-Hamid, H., and Ayoup, M. S. (2020). Two decades of recent advances of Ugi reactions: synthetic and pharmaceutical applications. *Rsc. Adv.* 10 (70), 42644–42681. doi:10.1039/d0ra07501a

Gokhale, K. M., and Telvekar, V. N. (2021). Novel peptidomimetic peptide deformylase (PDF) inhibitors of *Mycobacterium tuberculosis*. *Chem. Biol. Drug. Des.* 97 (1), 148–156. doi:10.1111/cbdd.13769

Hu, X., Nguyen, K. T., Jiang, V. C., Lofland, D., Moser, H. E., and Pei, D. (2004). Macrocyclic inhibitors for peptide deformylase: a structure–activity relationship study of the ring size. *J. Med. Chem.* 47 (20), 4941–4949. doi:10.1021/jm049592c

Joshi, T., Joshi, T., Sharma, P., Chandra, S., and Pande, V. (2021). Molecular docking and molecular dynamics simulation approach to screen natural compounds for inhibition of *Xanthomonas oryzae* pv. *Oryzae* by targeting peptide deformylase. *J. Biomol. Struct. Dyn.* 39 (3), 823–840. doi:10.1080/07391102.2020.1719200

Jung, D., Yum, S. J., Yu, Y. C., Kim, J. H., Lee, B. H., Jang, H. N., et al. (2016). Antimicrobial activities of actinonin against *Bacillus cereus*. *Korean J. Food. Sci. Technol.* 48 (6), 560–564. doi:10.9721/KJFST.2016.48.6.560

Kamada, H., Tsutsumi, Y., Sato-Kamada, K., Yamamoto, Y., Yoshioka, Y., Okamoto, T., et al. (2003). Synthesis of a poly(vinylpyrrolidone-co-dimethyl maleic anhydride) co-polymer and its application for renal drug targeting. *Nat. Biotechnol.* 21 (4), 399–404. doi:10.1038/nbt798

Kaur, A., Singh, B., and Jaggi, A. S. (2013). Synthesis and evaluation of novel 2, 3, 5-triaryl-4H, 2, 3, 3a, 5, 6, 6a-hexahydroindolo [3, 4-d] isoxazole-4, 6-diones for advanced glycation end product formation inhibitory activity. *Bioorg. Med. Chem. Lett.* 23 (3), 797–801. doi:10.1016/j.bmcl.2012.11.080

- Kong, C., Chee, C. F., Richter, K., Thomas, N., Abd. Rahman, N., and Nathan, S. (2018). Suppression of *Staphylococcus aureus* biofilm formation and virulence by a benzimidazole derivative, UM-C162. *Sci. Rep.* 8 (1), 2758. doi:10.1038/s41598-018-21141-2
- Kumar, H., Naithani, K., Bhalerao, P., Bhattacharya, B., and Bhowmik, S. (2023). Copper-catalysed one-pot cascade reaction strategy for the synthesis of benzoxazole-2-acrylic acid and benzoxazole-2 propanoic acid derivatives. *Tet. Lett.* 122, 154514. doi:10.1016/j.tetlet.2023.154514
- Kumar, S., Kanudia, P., Karthikeyan, S., and Chakraborti, P. K. (2014). Identification of crucial amino acids of bacterial peptide deformylases affecting enzymatic activity in response to oxidative stress. *J. Bacteriol.* 196 (1), 90–99. doi:10.1128/jb.00916-13
- Margolis, P. S., Hackbarth, C. J., Young, D. C., Wang, W., Chen, D., Yuan, Z., et al. (2000). Peptide deformylase in *Staphylococcus aureus*: resistance to inhibition is mediated by mutations in the formyltransferase gene. *Antimicrob. Agents Chemother.* 44 (7), 1825–1831. doi:10.1128/AAC.44.7.1825-1831.2000
- Marsh, J. A., and Teichmann, S. A. (2011). Relative solvent accessible surface area predicts protein conformational changes upon binding. *Structure* 19 (6), 859–867. doi:10.1016/j.str.2011.03.010
- Molteni, V., He, X., Nabakka, J., Yang, K., Kreusch, A., Gordon, P., et al. (2004). Identification of novel potent bicyclic peptide deformylase inhibitors. *Bioorg. Med. Chem. Lett.* 14 (6), 1477–1481. doi:10.1016/j.bmlc.2004.01.014
- O'Toole, G. A. (2011). Microtiter dish biofilm formation assay. *JoVE J. Vis. Exp.* 47, e2437. doi:10.3791/2437
- Park, S., Lee, J. H., Kim, Y. G., Hu, L., and Lee, J. (2022). Fatty acids as aminoglycoside antibiotic adjuvants against *Staphylococcus aureus*. *Front. Microbiol.* 13, 876932. doi:10.3389/fmicb.2022.876932
- Sargsyan, K., Grauffel, C., and Lim, C. (2017). How molecular size impacts RMSD applications in molecular dynamics simulations. *J. Chem. Theory Comput.* 13 (4), 1518–1524. doi:10.1021/acs.jctc.7b00028
- Scazzocchio, F., D'auria, F. D., Alessandrini, D., and Pantanella, F. (2006). Multifactorial aspects of antimicrobial activity of propolis. *Microbiol. Res.* 161 (4), 327–333. doi:10.1016/j.micres.2005.12.003
- Shahbaaz, M., Nkaule, A., and Christoffels, A. (2019). Designing novel possible kinase inhibitor derivatives as therapeutics against *Mycobacterium tuberculosis*: an *in silico* study. *Sci. Rep.* 9 (1), 4405. doi:10.1038/s41598-019-40621-7
- Swarupa, V., Chaudhury, A., and Sarma, P. V. G. K. (2018). Iron enhances the peptidyl deformylase activity and biofilm formation in *Staphylococcus aureus*. *3 Biotech.* 8, 32–38. doi:10.1007/s13205-017-1050-9
- Trott, O., and Olson, A. J. (2010). AutoDock Vina: improving the speed and accuracy of docking with a new scoring function, efficient optimization, and multithreading. *J. Comput. Chem.* 31 (2), 455–461. doi:10.1002/jcc.21334
- Van Der Spoel, D., Lindahl, E., Hess, B., Groenhof, G., Mark, A. E., and Berendsen, H. J. (2005). GROMACS: fast, flexible, and free. *J. Comput. Chem.* 26 (16), 1701–1718. doi:10.1002/jcc.20291
- Vashistha, A., Sharma, N., Nanaji, Y., Kumar, D., Singh, G., Barnwal, R. P., et al. (2023). Quorum sensing inhibitors as Therapeutics: bacterial biofilm inhibition. *Bioorg. Chem.* 106551, 106551. doi:10.1016/j.bioorg.2023.106551
- Walker, J. N., Flores-Mireles, A. L., Pinkner, C. L., Schreiber IV, H. L., Joens, M. S., Park, A. M., et al. (2017). Catheterization alters bladder ecology to potentiate *Staphylococcus aureus* infection of the urinary tract. *Proc. Natl. Acad. Sci. U. S. A.* 114 (41), E8721–E8730–E8730. doi:10.1073/pnas.1707572114
- Werneburg, G. T. (2022). Catheter-associated urinary tract infections: current challenges and future prospects. *Res. Rep. Urol.* Vol. 14, 109–133. doi:10.2147/RRU.S273663
- Wiegand, I., Hilpert, K., and Hancock, R. E. (2008). Agar and broth dilution methods to determine the minimal inhibitory concentration (MIC) of antimicrobial substances. *Nat. Protoc.* 3 (2), 163–175. doi:10.1038/nprot.2007.521
- Willekens, R., Puig-Asensio, M., Suanzes, P., Fernández-Hidalgo, N., Larrosa, M. N., González-López, J., et al. (2021). Mortality in *Staphylococcus aureus* bacteraemia remains high despite adherence to quality indicators: secondary analysis of a prospective cohort study. *J. Infect.* 83 (6), 656–663. doi:10.1016/j.jinf.2021.10.001
- Yang, S., Shi, W., Xing, D., Zhao, Z., Lv, F., Yang, L., et al. (2014). Synthesis, antibacterial activity, and biological evaluation of formyl hydroxyamino derivatives as novel potent peptide deformylase inhibitors against drug-resistant bacteria. *Eur. J. Med. Chem.* 86, 133–152. doi:10.1016/j.ejmech.2014.07.106
- Yoon, H. J., Kim, H. L., Lee, S. K., Kim, H. W., Kim, H. W., Lee, J. Y., et al. (2004). Crystal structure of peptide deformylase from *Staphylococcus aureus* in complex with actinonin, a naturally occurring antibacterial agent. *Proteins Struct. Funct. Bioinforma.* 57 (3), 639–642. doi:10.1002/prot.20231
- Zaghouani, M., Bögeholz, L. A., Mercier, E., Wintermeyer, W., and Roche, S. P. (2019). Total synthesis of (±)-fumimycin and analogues for biological evaluation as peptide deformylase inhibitors. *Tetrahedron* 75 (24), 3216–3230. doi:10.1016/j.tet.2019.03.037
- Zhong, Y., Zhou, L., Liu, X., Deng, L., Wu, R., Xia, Z., et al. (2021). Incidence, risk factors, and attributable mortality of catheter-related bloodstream infections in the intensive care unit after suspected catheters infection: a retrospective 10-year cohort study. *Infect. Dis. Ther.* 10, 985–999. doi:10.1007/s40121-021-00429-3